Chapter 1

Introduction and Literature Review

1.1 Introduction

Study of multiferroic materials, where the ferromagnetic (FM) or antiferromagnetic (AFM) and ferroelectric (FE) or antiferroelectric (AFE) phases coexist having coupled responses in a single phase material, are at the intense focus of researchers [Ramesh and Spaldin (2007); Eerenstein et al. (2006); Hill (2000); Khomskii et al. (2006); Tokura et al. (2006); Kimura (2003)(A)]. The simultaneous appearance and coupling of magnetization (M) and electric polarization (P) in a monophasic multiferroic materials exhibits very interesting physical properties and can offer the possibilities of new multifunctional sensors, actuators and data storage devices [Fiebig (2005); Khomskii (2006); Scott (2007); Wang et al. (2009)]. Multiferroic behaviour in single phase materials is rare in nature due to contradictory requirements of electronic structure. Occurrence of magnetism generally requires partially filled d-orbitals while presence of ferroelectricity requires empty d-orbitals [Hill (2004), Wang et al. (2009)]. Most of the known single phase multiferroic materials have either very weak responses or have multiferroic behaviour at extremely below the room temperature, making them practically useless for device applications [Hill (2004)]. Among various interesting single phase multiferroic materials, the $BiFeO_3$ has attracted intense research interest because it is the only room temperature multiferroic having both the ferroelectric and antiferromagnetic transition temperatures above room temperature [Wang et al. (2003), Fiebig (2005)]. However, the limitation with the $BiFeO_3$ is that its G-type antiferromagnetic state has spin spiral structure sue to which the weak ferromagnetism due to spin canting is not observed and the linear magnetoelectric effect averages to zero. To observe the linear magnetoelectric effect in $BiFeO_3$, the spiral spin structure needs to be broken. It has been reported that spiral spin

structure of $BiFeO_3$ can be destroyed by application of intense magnetic field of ~ 20 kOe [Popov et al. (1993)]. However, a more convenient way to destroy the spin spiral structure of $BiFeO_3$ for observing linear magnetoelectric effect is by chemical substitutions at Bi and Fe sites. Solid solution formation of $BiFeO_3$ with several other perovskites like $PbTiO_3$, $BaTiO_3$, $Pb(Fe_{0.5}Nb_{0.5})O_3$ etc. have been investigated in recent years to develop promising multiferroic materials [Bhattacharjee et al. (2013), Singh et al. (2008)C, Singh et al. (2013), Patel et al. (2013)]. The present thesis deals with the investigation of a new multiferroic solid solution of $BiFeO_3$ with $Sr(Fe_{0.5}Nb_{0.5})O_3$ and its characterization for crystal structure, magnetic, ferroelectric and dielectric behaviour as a function of composition and temperature. This chapter presents the basic definitions, general introduction of ferroelectricity and magnetism along with the discussion on various concepts required for understanding of multiferroic phenomenon. Further, it is followed by a brief review of existing literature on multiferroic materials. The literature on $BiFeO_3$ based multiferroic solid solutions and $Sr(Fe_{0.5}Nb_{0.5})O_3$ is reviewed at the end of this chapter.

1.2 General Description of the Perovskite Structure

Perovskite is a calcium titanium oxide mineral with chemical formula ($CaTiO_3$). This compound was first discovered by Gustav Rose in 1839 and is named after Russian mineralogist, L. A. Perovski [1792-1856]. The family of compounds that have crystal structure similar as $CaTiO_3$, are called as the perovskites materials. The ideal perovskite compounds have general chemical formula as ABO_3, where the letters ‘A’ and ‘B’ stand for the two cations with total ionic charges as +6 and ‘O’ is generally a divalent anion like oxygen. The cation A is generally monovalent, divalent or trivalent while the cation B is generally divalent, trivalent, tetravalent, pentavalent or hexavalent with partial occupancy with another lower valence cation. The A and B sites can accommodate

single or multiple cations with total valence of +6, without disturbing the perovskite structure. In ABO_3 perovskite structure B cation shows a 6-fold coordination i.e. octahedral coordination while cation 'A' has 12-fold i.e. cuboctahedral coordination. The cubic crystal system with *Pm*-3*m* space group (space group no. 221) is the ideal perovskite structure in which 'A' cation occupies the (0, 0, 0) positions on the 1(a) Wyckoff site, 'B' cation occupies the (1/2, 1/2, 1/2) positions on the 1(b) Wyckoff site, whereas the 'O' anion occupies the (1/2, 1/2, 0) positions on the 3(c) Wyckoff site. Figure 1.1(a) and 1.1(b) shows the two schematic sketches for the cubic perovskite structure. The relative ionic radii of the cations and anions constituting the perovskite structure decide if it will crystallize in perovskite structure or not. The stability and degree of distortion of a real perovskite structure from its ideal cubic structure is measured using following expression suggested by Goldschmidt [V. M. Goldschmidt, Die Gesetze der Krystallochemie. Naturwissenschaften 14, 477-485 (1926)] also called as tolerance factor 't'

$$t = \frac{R_A + R_O}{\sqrt{2}(R_B + R_O)} \qquad \text{…….. ……..} \quad (1.1)$$

where, 'R_A', 'R_B' denote the ionic radii of cations 'A' and 'B' and 'R_O' denotes the same for anion 'O'. If the value of 't' becomes equal to 1, the perovskite structure is expected to adopt the ideal cubic symmetry. If the ionic radius of atom 'B' at the oxygen octahedron position is so small that gives the value of 't' > 1, the structure get distorted and causes a small polarisation as in $BaTiO_3$. If for a perovskite structure the value of 't' is slightly less than unity, the tilting and the rotation of the oxygen octahedral becomes favourable as observed in $CaTiO_3$.

However, for those compounds such as $LiNbO_3$ having the value of 't' very small, a strongly distorted structure with only 6 neighbours for the 'A' cation is

favoured. If the value of the 't' is very different from unity, the perovskite type structures will be unfavourable. For a stable perovskite structure, the value of 't' should normally lie in the range of $0.80 < t < 1.05$.

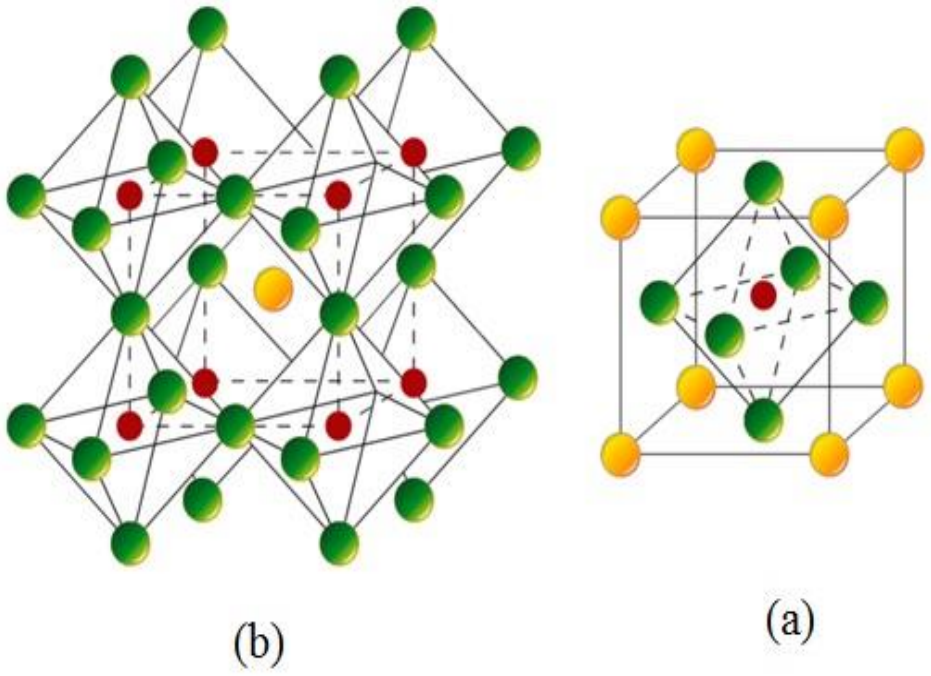

Figure 1.1 Two typical view of the cubic perovskite structure (a) cation 'A' sits on the cubic corner position (0, 0, 0) (shown by big yellow sphere), B cation sits on the (1/2, 1/2, 1/2) position (shown by small red sphere) and O anion sits on the face diagonal (1/2, 1/2, 0) positions (shown by medium size green sphere) (b) perovskite structure represented in the form of connected BO_6 octahedra, A cation is shown by the big yellow sphere, B cation is shown by the small red sphere while the O anion is shown by the green spheres.

1.3 Ferromagnetic and Antiferromagnetic Materials

The materials which have spontaneous magnetisation in the absence of external magnetic field and the direction of magnetisation can be changed hysterically

by the application of external magnetic field are known as ferromagnetic materials. In such materials there exist an internal molecular field that causes the alignment of magnetic moments parallel to each other which leads to the spontaneous magnetisation. The molecular field has been found to be originated from quantum mechanical exchange energy that forces electrons with parallel spins (and hence parallel magnetic moments) to a lower energy state than those with antiparallel or random spins [B.D. cullity (1972)]. The degree of the alignment of the spins (atomic magnetic moments) in the ferromagnetic materials decreases with the increase of temperature. This means that thermal energy make them disordered and the ferromagnetic materials transform to a paramagnetic one at higher temperatures. The temperature at which ferromagnetic materials transform to paramagnetic is known as the Curie temperature (T_C). Above the transition temperature (T_C) the magnetic susceptibility follows the Curie-Weiss law written as

$$\chi = \frac{C}{T - T_C} \qquad \text{.....(1.2)}$$

It is found that as-prepared samples of ferromagnetic materials often show a lack of macroscopic magnetization. This is due to the random orientation of various domains of magnetization present in the materials to minimize the energy of the system. The application of external magnetic field (H) causes reorientation and subsequent alignment of the domains that lead to hysteresis in the magnetization (M) and applied magnetic field (H) as shown in Fig. 1.2. When the magnetic moments of neighbouring atoms arrange themselves antiparallel to each other, it is termed as antiferromagnetism**.** In this case, the resultant magnetic moment becomes zero because of the total cancellation of both spin and orbital moments. Depending on the crystal lattices on which an equal number of up and down spins are to be arranged, antiferromagnetic orderings are categorised as (A-, C-, G-, or E-type) [Wollan et al. (1955)]. The

temperature above which antiferromagnetic ordering vanishes is known as the Neel temperature (T_N). Above Neel temperature (T_N), the material behaves like a typical paramagnet.

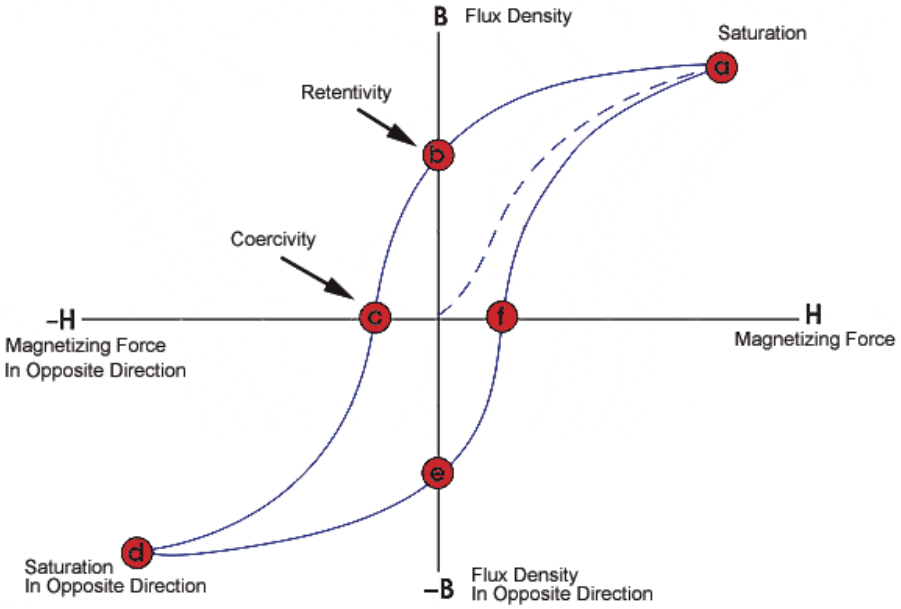

Figure 1.2 Typical M-H hysteresis loop for a ferromagnetic material [after Cullity (1972)].

Below T_N, the energy of antiparallel ordering of neighbouring spins dominates over the thermal energy and this established an antiferromagnetic state. Above T_N, for antiferromagnet, the variation of inverse susceptibility (χ^{-1}) with temperature also traces a straight line, just like paramagnetic state of ferromagnets, but in this case line extrapolates to negative Curie temperature ($-T_C$) at $1/\chi = 0$. Above T_N, it obeys the Curie-Weiss law. Although, one does not expect net magnetization in the antiferromagnetic materials, it may exhibit net magnetization due to spin canting, lattice defects, and, frustrated surface spins in the absence of magnetic field. The application of sufficiently high magnetic field may rotate the spin direction of one of the magnetic sub-lattices and eventually leads to the 'spin flop' where all the spins would be aligned

in a parallel fashion. At sufficiently high magnetic fields, the spin direction of one of the magnetic sublattices may rotate and eventually lead to the 'spin flop' where all the spins would be aligned in a parallel fashion. Thus the application of external magnetic field can induce magnetisation in the system by rotation and spin flop.

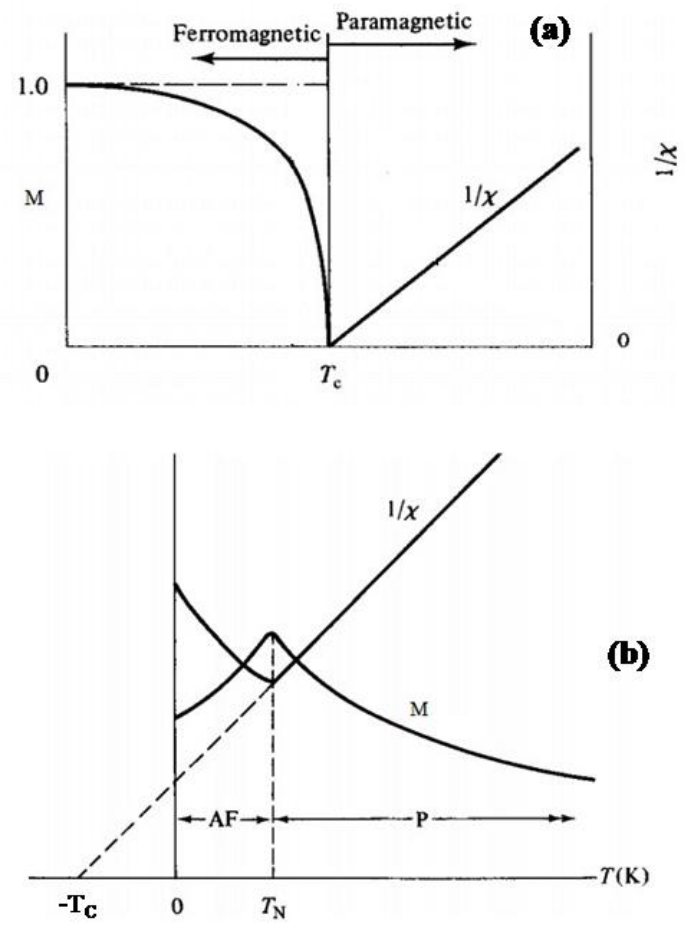

Figure 1.3 Temperature dependence of the magnetization (M) and inverse of the magnetic susceptibility (χ^{-1}) for (a) ferromagnetic and (b) antiferromagnetic material. AF = Antiferromagnetic and P = Paramagnetic [after Cullity (1972)].

The variation of magnetisation (M) and inverse susceptibility (χ^{-1}) with temperature for different types of magnetic materials (ferromagnetic and antiferromagnetic) are depicted in Fig. 1.3 (a) and (b).

1.4 Magnetic Exchange Interactions

There are different types of magnetic materials in which magnetic moments interact one other and the interaction between moments are termed as magnetic interactions. This is a quantum mechanical phenomenon and is also known as exchange interaction mediated by the overlapping of electronic wave function in conjunction with Pauli's exclusion principle. The nature of the magnetic exchange interactions among the magnetic moments justifies whether the material is ferromagnetic or antiferromagnetic. Now, we shall discuss various kinds of magnetic exchange interactions that establish the long range magnetic order state.

1.4.1 Direct Exchange Interaction

The term direct exchange interaction is used for those interactions which are mediated between the neighbouring magnetic ions. If we consider two atoms 'i' and 'j' having spin angular momentum $S_i(h/2\pi)$ and $S_j(h/2\pi)$ respectively, then the exchange interaction energy between them is given by the expression

$$E_{ex} = -2J_{ex}\, S_i.S_j = -2J_{ex}\, S_i.S_j \cos\varphi \qquad \ldots\ldots\ldots\ldots\ldots\ldots\ldots\ldots\ldots\ldots \quad (1.3)$$

Where, J_{ex} is known as exchange integral, and φ is the angle between the spins S_i and S_j. The positive value of J_{ex} and parallel spin ordering ($\cos\varphi = 1$) drive the system in lower energy E_{ex} state while antiparallel spin ordering ($\cos\varphi = -1$) drive the system in higher energy state. But the case will be opposite with negative value of J_{ex} (i.e. the exchange energy of the system E_{ex} will be lower with antiparallel spin ($\cos\varphi = -1$) and higher with parallel spin ($\cos\varphi = 1$) configuration). If J_{ex} is negative, the lowest energy state will result from antiparallel spins. A positive value of the exchange integral is, therefore, a necessary condition for ferromagnetism to occur. The behaviour of direct exchange interaction can be described using the Bethe-Slater curve shown in Fig. 1.4

which represents the magnitude and sign of exchange integral (J_{ex}) as a function of inter-atomic distance.

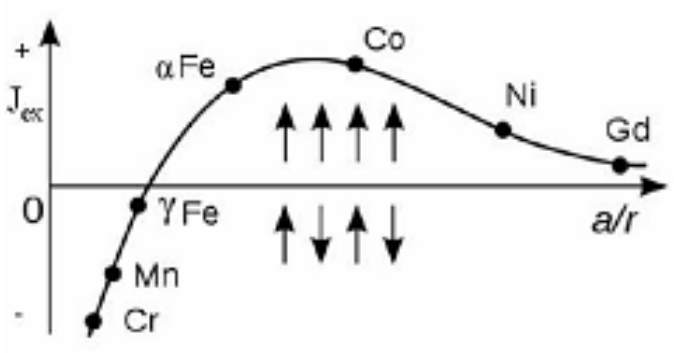

Figure 1.4 Bethe-Slater curve (schematic). 'a' is the radius of an atom and "r' the radius of its 3d shell of electrons [after Cullity (1972)].

1.4.2 Indirect Exchange Interaction

The exchange interaction between magnetic ions mediated by a non-magnetic ion is known as indirect exchange interaction. The super exchange and double exchange are two main examples of the indirect exchange interactions. Both the interactions are strongly dependent on the magnetic moment of the magnetic ions, the overlap integral between the orbitals of magnetic ions and anions, and the bond angle between the two magnetic ions.

1.4.3 Super Exchange Interaction

The interaction between the magnetic moments of ions that are too far apart to be influence by direct exchange, are described by super exchange interaction which leads to antiferromagnetic ordering. In this type of interactions magnetic ions of same valence are coupled by a non-magnetic ion placed in between them [Anderson (1950)]. MnO and MnF_2 are the best examples of antiferromagnetic system in which the magnetic moments of Mn^{2+} ions interact by the mechanism of super exchange

interaction because, in each system, the direct overlapping of wave functions of electrons on the two Mn^{2+} ions does not exist. For a perfectly ionic system, each magnetic ion would contain a singly filled d-orbital whereas oxygen anion would have two p-electrons in its outer most occupied states. The strength of antiferromagnetic coupling between the magnetic ions (M) determined by the bond angle M-O-M and is generally greatest when this angle is 180˚ (M-O-M collinear).

1.4.4 Double Exchange Interaction

There are some oxide materials in which magnetic ions have mixed valency i.e. it can exist in more than one oxidation state. In the mixed manganite system such as $La_{1-x}Sr_xMnO_3$, manganese ion can exist in the oxidation states 3 or 4, i.e. as Mn^{3+} or Mn^{4+}. The ferromagnetic alignment is observed in such system which is mediated by the double exchange mechanism proposed by Zener [Zener (1951)]. According to Zener (1951) the intra-atomic Hund's rule exchange is stronger and the carriers taking part in hoping process from one ion to the next do not change their spin direction. This means that hoping of charge carriers is possible only if the spin orientations of the two ions are parallel. Now we take an example of linear (180˚) interaction of Mn-O-Mn in which the "e_g" orbitals of manganese ion are directly interacting to the "2p" orbitals of oxygen (O^{2-}) and one manganese ion (Mn^{3+}) contains more electron than other (Mn^{4+}). In the ground state, electrons on each manganese ion are configured in accordance with Hund's rule. If oxygen (O^{2-}) ion releases its electron with up spin for Mn^{4+} ion, this vacancy of electron in O^{2-} is filled by an electron from Mn^{3+}. At the end of the process, an electron has moved between the neighbouring metal ions, retaining its spin. The double exchange mechanism predicts that the electronic transformation between two species will happen more easily if it preserves its spin orientation at the time when it is on the accepting species. The hoping ability of electron from one species to another

reduces the kinetic energy of the system and favours the ferromagnetic alignment of neighbouring magnetic moments. This model seems to be similar to the superexchange. However, in the case of superexchange, the interacting ions are in same oxidation states while in double exchange interaction one ion has an extra electron than the other i.e. ions taking part in the interaction are in different oxidation states. A schematic representation of double exchange mechanism is depicted in Fig.1.5.

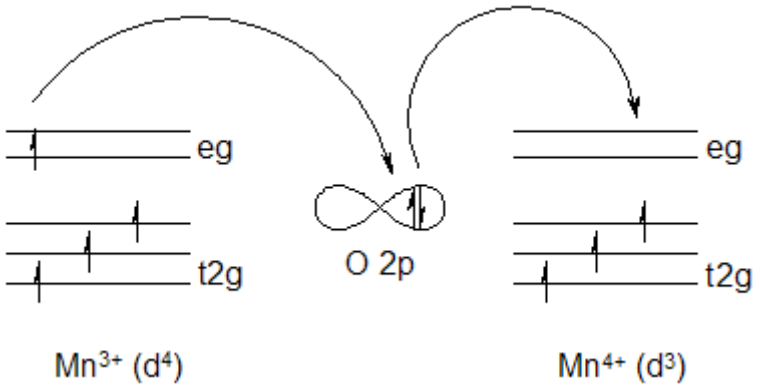

Figure 1.5 Double exchange mechanism gives ferromagnetic coupling between Mn^{3+} and Mn^{4+} ions participating in electron transfer [after Singh Ranber (2013)].

1.4.5 Anisotropic Super-Exchange Interaction

To include the contribution coming from spin-orbit coupling a new theory was developed and termed as anisotropic superexchange interaction which is the extension of Anderson theory of super exchange interactions including spin-orbit interaction also. Some antiferromagnetic systems consist of magnetic moments that are not exactly antiparallel to each other but they are canted with respect to each other. Such canted magnetic moments may induce weak ferromagnetic moment. Spin canting requires two contributions: (1) the presence of two non symmetry related nearest-neighbour magnetic ions and (2) anti-symmetric exchange and/or single ion anisotropy. Anti-symmetric exchange is based solely upon symmetry arguments shown by Dzyaloshinskii

[Dzyaloshinskii (1958)], while [Moriya (1960)] is credited with determining the mechanism by which individual spins interact via spin-orbit coupling and the relation between single-ion anisotropy and the magnitude of the interaction. These two arguments resulted in the anisotropic exchange interaction that is commonly known as the Dzyaloshinskii-Moriya (DM) interaction. The DM interaction is given by the Hamiltonian [Moriya (1960)] as $H_{D\text{-}M} = \mathbf{D}_{12}.|\mathbf{S}_1 \times \mathbf{S}_2|$, where, $\mathbf{D}_{12}$ is called DM vector and it vanishes in the presence of inversion symmetry of the crystal field with respect to the centre between the two magnetic ions. The origin of DM interaction is caused by the interplay between super-exchange and spin-orbit coupling. DM interaction reduces the coupling energy of the system by canting of the spins S_1 and S_2. Since magnitude of $\mathbf{D}_{12}$ depends on (g-2)/g, where 'g' is Lande's g-factor, it is obvious that, as 'g' departs significantly from 2, the anisotropy is large and spin canting becomes dominant.

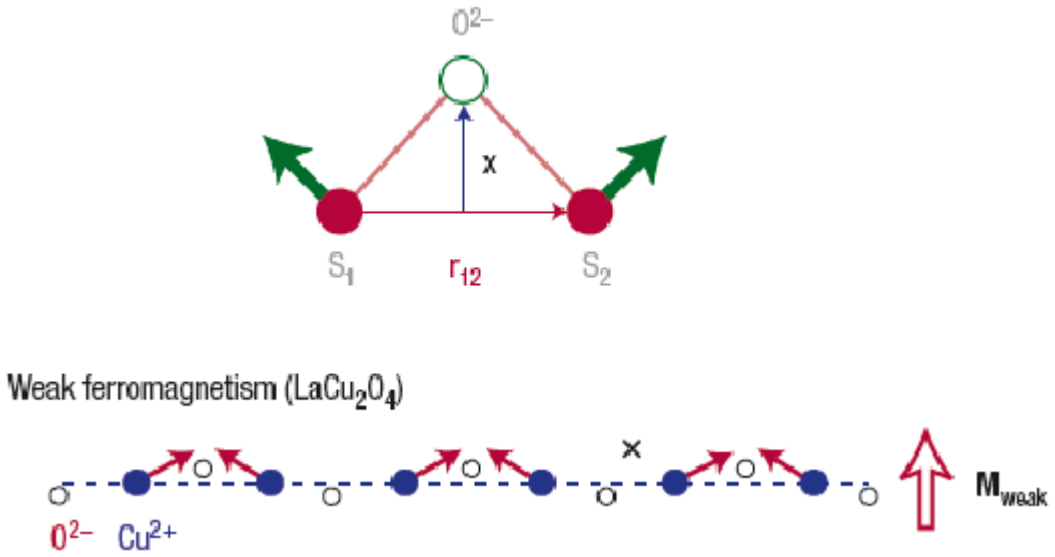

Figure 1.6 Consequences of Dzyaloshinskii-Moriya (DM) interaction. Weak ferromagnetism in antiferromagnet La_2CuO_4 layers results from the alternating Dzyaloshinskii vector [After Cheong et al. (2007)].

It is also proportional to the position of oxygen between the two magnetic ions i.e. $\mathbf{D}_{12} \propto \boldsymbol{x} \times \mathbf{r}_{12}$ where, $\mathbf{r}_{12}$ is the vector connecting the two magnetic ions and $\boldsymbol{x}$ is the perpendicular displacement of oxygen from this vector. The DM interaction favours non-collinear spin ordering. For example, the appearance of weak ferromagnetism in La_2CuO_4 system is the results of spin canting caused by DM interaction. The schematic spin arrangements in La_2CuO_4 due to DM interaction are shown in Fig. 1.6.

1.5 Ferroelectricity and Antiferroelectricity

Some materials have spontaneous polarisation (P_S) whose direction can be reversed on application of an external electric field. Such materials are called ferroelectric and this phenomenon is called ferroelectricity. The polar group of crystals that are non-centrosymmetric usually exhibit the phenomenon of ferroelectricity [Jaffe et al. (1971)]. All the ferroelectric materials show two characteristic features: (i) they exhibit polarisation (P) versus externally applied electric field (E) hysteresis loop similar to that shown in Fig. 1.7, because of domain formation similar to ferromagnetic materials. As temperature of these materials increases the area of hysteresis loop decreases and disappear at a certain temperature called Curie point (T_0). (ii) Above the Curie temperature i.e. the state is said to be paraelectric and the variation of dielectric permittivity (ε_r) with temperature is governed by the Curie-Weiss law given as,

$$\varepsilon_r = \frac{C}{T - T_C} \qquad \text{..... (1.4)}$$

Where, ε_r is the real part of the dielectric permittivity of the material and T_C is the Curie temperature. The Curie temperature (T_C) can be calculated by the extrapolation of temperature dependent inverse permittivity ($1/\varepsilon_r$) plot. The values of Curie temperature (T_C) and Curie point (T_0) tells about the order of ferroelectric phase transition. In the case of first order transition (characterizes by discontinuous change in lattice parameters, polarisation etc.) T_C is lower than T_0 [Lines and Glass (1977)] while if it is

second order (characterizes by continuous change in lattice parameters, polarisation etc.) both are equals i. e. $T_C = T_0$.

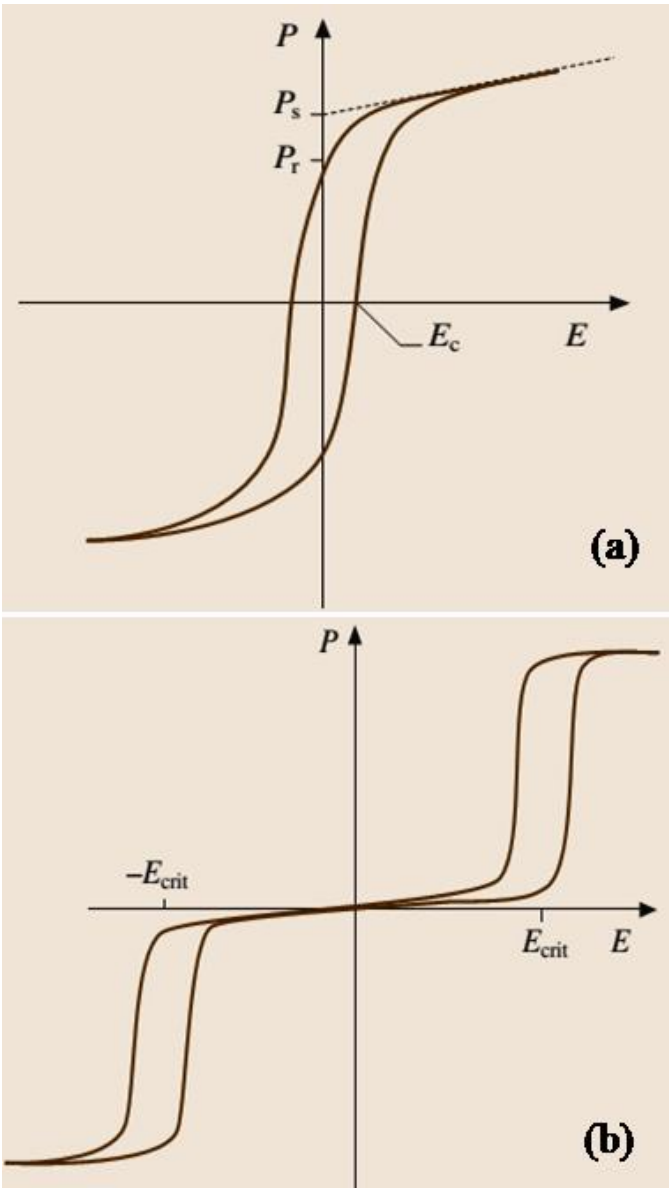

Figure 1.7 Typical hysteresis loop for (a) ferroelectric and (b) antiferroelectric materials (after Martienssen and Warlimont (2005)).

There are class of materials that have sublattice polarizations but show the absence of spontaneous macroscopic polarization. These materials are known as antiferroelectric (AFE) materials. The antiferroelectric materials consist of electric dipole moments

aligned antiparallel to each other. The arrangement of these dipoles in antiferroelectrics can be visualized as two polarized sub-cells oriented in opposite sense causing a centre of symmetry that lead to a net zero macroscopic polarization. However, if these materials are placed in a region of sufficiently high electric field, a macroscopic polarization can be induced. Unlike FE materials, they exhibit "twin" polarisation (P) versus electric field (E) (i.e. P-E) hysteresis loops as depicted in Fig. 1.7. $PbZrO_3$ [Jona (1957)] and $NaNbO_3$ [Cross and Nicholson (1955)] are the best known examples of the antiferroelectric materials. The antiferroelectric phase transition is caused by equal but opposite displacements of a pair of ions. Due to this type of ionic displacements, the unit cell of antiferroelectric phase becomes multiple of the prototype paraelectric phase and gives rise to the appearance of characteristic superlattice reflections in the diffraction pattern. Antiferroelectric materials also show a transition temperature above which they transform to paraelectric state. In analogy with antiferromagnetic materials, the transition temperature for the antiferroelectric material is commonly known as Neel temperature.

1.6 Magnetoelectric Coupling in Multiferroic

The monophasic multiferroic materials having coupled electric and magnetic order parameters generally exhibit the appearance of polarisation (P) on application of magnetic field (H) and magnetisation (M) on the application of electric field (E). This phenomenon is termed as magnetoelectric effect. In the view of thermodynamics, magnetoelectric effect in monophasic crystal is traditionally described in the frame work of Landau theory by writing the free energy (F) expression of the system in terms of an applied magnetic field (**H**) whose i^{th} component is designated by H_i and an applied electric field (**E**) whose i^{th} component is designated by E_i [Fiebig (2005); Wang et al. (2009)]:

$$F(E,H) = F_0 - P_i^s E_i - M_i^s H_i - 1/2\varepsilon_0\varepsilon_{ij}E_iE_j - 1/2\mu_0\mu_{ij}H_iH_j - \alpha_{ij}E_iH_j - 1/2\beta_{ijk}E_iH_jH_k - 1/2\gamma_{ijk}H_iE_jE_k - \quad \text{.....(1.5)}$$

where, F_0 is the ground state free energy, subscripts (i, j, k) refer to the three components E_i and H_i, the components of the electric field E and magnetic field H, respectively; P_i^s and M_i^s denote the components of spontaneous polarization P^S and magnetization M^S, ε_0 and μ_0 are the dielectric and magnetic susceptibilities of vacuum, ε_{ij} and μ_{ij} are the electric and magnetic susceptibilities respectively. The coefficient α_{ij}, a second rank tensor which corresponds to induction of polarization by a magnetic field or of magnetization by an electric field, is designated as the linear magnetoelectric effect. β_{ijk} and γ_{ijk}, are third rank tensors, representing higher order (quadratic) magnetoelectric coefficients. The differentiation of equation (1.5) w.r.t. E_i or H_i and then setting E_i or H_i =0 leads to magnetoelectric effect in the form of $P_i(H_i)$ or $M_i(E_i)$ that is given as:

$$P_i = \alpha_{ij}H_j + \frac{\beta_{ijk}}{2}H_jH_k + \quad \text{.....(1.6)}$$

$$\mu_0 M_i = \alpha_{ij}E_j + \frac{\gamma_{ijk}}{2}E_jE_k + \quad \text{..... (1.7)}$$

The ability of coupling the magnetic and the electric order parameters in magnetoelectric multiferroics provides an extra degree of freedom in the design of actuators, transducers, and storage devices. Such magnetoelectric multiferroics are suggested to have potential for designing some specific device applications that include transducers with magnetically modulated piezoelectricity, multiple state memory elements (corresponding to +P, -P, +M and -M states), electric-field controlled ferromagnetic resonance devices [Fiebig (2005); Ramesh and Spaldin (2007); Wang etal. (2009)] etc.

1.7 Incompatibility between Ferroelectricity and Magnetism

The single phase materials having coupled ferroelectric and magnetic orders have not only interesting application oriented properties [Fiebig (2005)] but, due to the existence of rich physics, they offer interesting challenges to condensed matter theorists also. It has been found that the appearance of ferroelectricity in ABO_3 perovskites caused by the off-centering displacement of B-site transition metal (TM) cations (such as Ti^{4+} in $BaTiO_3$) needs empty d orbitals (d^0 electrons) for the hybridization of 3d Ti and 2p O orbitals [Cohen (1992)(A)]. Further, the absence of spatial inversion symmetry is essential for the generation of ferroelectricity; while in contrast, for the existence of magnetism transition metal ion with partially filled d orbital and the breaking of the time reversal symmetry is required [Pandey and Singh (2009)]. The two phenomena, which thus appear to be mutually exclusive, have nevertheless been found to coexist in a small number of magnetoelectric multiferroics which should exhibit asymmetry in space and time both [Pandey and Singh (2009)]. This implies that in magnetoelectric materials, the ferroelectric distortion is not caused by the hybridization of transition-metal ions in a noble gas configuration.

1.8 Mechanism for Coexistence of Ferroelectricity and Magnetism

As stated above, the ferroelectric materials with general formula ABO_3 require empty d^0 orbitals of B-site transition metal (TM) ions to establish the hybridization with surrounding anions. This type of electronic structure is normally expected to exclude magnetism. However, there are few materials which exhibit both types of behaviour mostly due to secondary effect or some other mechanisms. To explain this discrepancy new mechanisms for the origin of ferroelectricity and magnetisation have been proposed in recent years for materials that allow the mutually exclusive phenomena

(ferroelectricity and magnetism) to occur in the same phase as discussed in the following sections.

1.8.1 Mixed Occupancy of the Magnetic Transition Metal (TM) Ions (d^n) with Ferroelectrically Active TM (d^0) Ions

First of all Russian researchers initiated the study of multiferroic perovskites and suggested for the mixing of magnetic transition metal (TM) ions having partially filled (d^n) orbitals with ferroelectrically active TM ions containing empty (d^0) orbitals at B-site. It was expected that such mixing (partially filled (d^n) magnetic TM ions and empty d^0-shell TM ions) on the B-site will separately lead to a magnetic order and a ferroelectric order in the same material. Fortunately, the idea has become successful and the coexistence of electric and magnetic order was reported in perovskite such as $Pb(Fe_{1/2}Nb_{1/2})O_3$ (PFN) in which Fe^{3+} ions are magnetically active and Nb^{5+} ions are ferroelectrically active [Fiebig et al. (2005), Wang et al. (2009), Singh et al. (2010)(A)]. Further, theoretical predictions along with experimental results have confirmed the ferroelectric Curie temperature of ~ 385 K [Plantov et al. (1970)] and magnetic Neel temperature of ~ 143 K [Bokov et al. (1962), Bhatt et al. (2004)] for this compound.

1.8.2 Ferroelectricity Induced by ns^2 Lone Pair of Electrons

In some ABO_3 type perovskite materials the cations sitting at A-site consists of a $(ns)^2$ lone pair valence electron configuration. Such configuration of lone pair electrons on the cations is unstable and has tendency to mix its $(ns)^2$ ground state with a low-lying $(ns)^1$ $(np)^1$ excited state. This forces the ions (containing the lone pair of electrons) to lose the inversion symmetry [Atanasov (2001)] and hence causing the off-centre distortion which in turn induce ferroelectricity [Hill (2000)]. The lone pair induced ferroelectricity are reported in some Bi-based compounds like $BiFeO_3$ and $BiMnO_3$, where magnetic properties are governed by B-site ions and ferroelectricity is

driven by lone pair mechanism of A-site ions [Wang et al. (2003); Hill (2000)]. In the family of perovskite materials that show lone pair electron induced ferroelectricity, $BiFeO_3$ is unique because it shows the multiferroicity at room temperature and has extremely high magnetic (T_N ~ 643 K) and ferroelectric (T_C ~ 1103 K) transition temperatures.

1.9 Multiferroic Materials with Improper Ferroelectricity

In the multiferroic materials discussed in the preceding sections, the ferroelectric transition is mainly driven by the crystallographic structural instability towards the polar state where polarization (P) plays the role of primary order parameter. Such kinds of materials are commonly known as 'proper' ferroelectrics. If on the other hand, the origin of ferroelectricity in materials is governed by the magnetic transitions or is a by-product of complex lattice distortion, such materials are classified as 'improper' ferroelectrics [Levenyuk et al (1974); Cheong et al. (2007)]. In this class of materials ferroelectricity is not driven by the conventional mechanism of structural phase transition where polarisation (P) is the primary order parameter. We have listed in Table 1.1 some examples of improper ferroelectrics reported in the literature.

Table 1.1 Classification of ferroelectrics [after Cheong et al. (2007)]

	Mechanism of inversion symmetry breaking	Materials
Proper	Covalent bonding between $3d^0$ transition metal (Ti) and oxygen	$BaTiO_3$
	Polarization of $6s^2$ lone pair of Bi or Pb	$BiMnO_3$, $BiFeO_3$, $Pb(Fe_{2/3}W_{1/3})O_3$
Improper	Structural transition 'Geometric ferroelectrics'	K_2SeO_4, Cs_2CdI_4 hexagonal $RMnO_3$
	Charge ordering 'Electronic ferroelectrics'	$LuFe_2O_4$
	Magnetic ordering 'Magnetic ferroelectrics'	Orthorhombic $RMnO_3$, RMn_2O_5, $CoCr_2O_4$

1.9.1 Geometric ferroelectricity in Hexagonal manganites

The origin of ferroelectricity in rare-earth hexagonal manganites having general chemical formula as $RMnO_3$ (R is the rare-earth element such as Lu, Ho or Y) is attributed to be the by-product of a complex lattice distortion [Aken et al. (2004)]. In this group of manganites, $YMnO_3$ is the most studied one. From the structural point of view, it consists of non-connected layers of MnO_5 trigonal bipyramids corner-linked by in-plane oxygen (O_p), with apical oxygen ions (O_T) forming close-packed planes separated by a layer of Y^{3+} ions. In order to attain a closed packing (as generally occur in case of perovskite ABO_3 when the A-site ions is very small) at ferroelectric transition, the layered structure and the triangular symmetry of this compound forces to rotate the MnO_5 polyhedral that, in turns, along with lowering the symmetry also eliminate the inversion centre and establishes a ferroelectric state that comprises most of the dipole moments formed by 'Y-O' pairs [Aken et al. (2004)]. Here, it has to be emphasized that the origin of ferroelectricity in perovskites is not possible by above process of BO_6 tilting. All the compounds belonging to this class of manganites show triangular layer type magnetism with T_N in the range 50-100 K.

1.9.2 Ferroelectricity Induced by Charge Ordering

In the charged ordered system ferroelectricity is induced by the electronic correlation rather than the covalency. In a number of doped ABO_3 type manganites localization of charge carriers at low temperature set up a periodic but non-symmetric charge ordered (CO) structure. This asymmetrical ordering of charge induces improper ferroelectricity in these systems, as in the case of $Pr_{1-x}Ca_xMnO_3$ [Brink et al. (2008); Efermov et al. (2004); Ederer et al. (2004)]. In the bilayer manganite such as $Pr(Sr_{0.1}Ca_{0.9})_2Mn_2O_7$ a charge ordering induced polar lattice distortion has been also

reported. Magnetic ordering in these manganites is accompanied with the appearance of improper ferroelectricity below the charge ordering temperature.

1.9.3 Ferroelectricity Induced by Spiral Spin Ordering

In some magnetoelectric multiferroics, spins configure themselves in spiral geometry that may spontaneously breaks time-reversal as well as inversion symmetry. The lack of inversion centre in such systems occurs because changing the sign of all coordinates, inverts the direction of rotation of spins in the spiral. Thus the symmetry of spin spiral plays the major role for the origin of electric polarisation in such systems. The sign of electric polarisation thus induced is determined by the direction of the rotation of spin. The microscopic mechanism causing electric polarisation includes the antisymmetric Dzyaloshinskii-Moriya (DM) interaction written as $D_{m,m+1} . (S_m \times S_{m+1})$, where, $D_{m,m+1}$ is the Dzyaloshinskii vector [Moriya (1960), Dzyaloshinskii (1964)]. This interaction is the result of relativistic correction to the usual super-exchange interaction. Strength of this interaction is directly proportional to the degree of spin-orbit coupling. The vector '$D_{m,m+1}$' is proportional to the vector product of the unit vector ($r_{m,m+1}$) in the direction of line joining the magnetic ions 'm' and 'm+1' and the displacement vector '*x*' of the oxygen anion from this line i.e. $D_{m,m+1} \propto (x \times r_{m,m+1})$ (see Fig. 1.8). This implies that any change in the value of '*x*' causes the corresponding change in the DM interaction energy which further determines the degree of inversion symmetry breaking at the oxygen site.

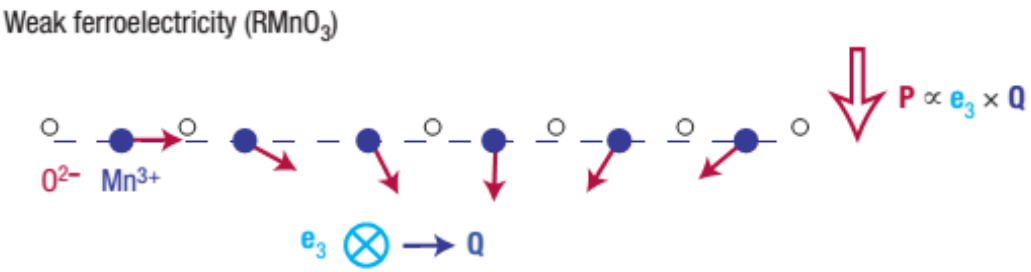

Figure 1.8 Weak ferroelectricity induced by the exchange-striction effect in the magnetic spiral state, which forces to shift the oxygen anion in one direction normal to the spin chain constituted by the magnetic ions [after Cheong et al.(2007)].

Due to the same sign of vector product ($S_m \times S_{m+1}$) for all neighbouring spin pairs, DM interaction forces to shift the oxygen anion in certain direction normal to the spin chain constituted by the magnetic ions and thus induces the electric polarisation normal to the chain [Sergienko I. A. &Dagotto E. (2006)]. The induced electric polarisation is governed by $P_{m,m+1} \propto r_{m,m+1} \times (S_m \times S_{m+1})$ [Katsura, H., 2005]. The multiferroicity in compounds like $RMnO_3$ (R = Tb, Gd) and RMn_2O_5 (R = Tb, Y) are governed by this mechanism. Among these compounds $TbMnO_3$ is unique that has been reported to show the largest value of pressure induced spin- driven ferroelectric polarization (≈ 1.0 μC/cm^2) that is further enhanced to (≈ 1.8 μC/cm^2) on application of external magnetic field [Aoyama et al. (2014)] .

1.10 Structure and Multiferroic Properties of $BiFeO_3$

At ambient temperature bismuth ferrite ($BiFeO_3$) crystallises in a rhombohedrally distorted perovskite structure in *R*3*c* space group [Jacobson et al. (1975); Fischer et al. (1980); Kubel (1990); Sosnowska et al. (2002)]. The hexagonal unit cell is chosen in the rhombohedral structure for ease of structural analysis that gives

the lattice parameters of $BiFeO_3$ as a = b = 5.58102(4), c = 13.8757(4), $\alpha = \beta = 90^0$ and $\gamma = 120^0$ [Palewicz et al. (2007)].

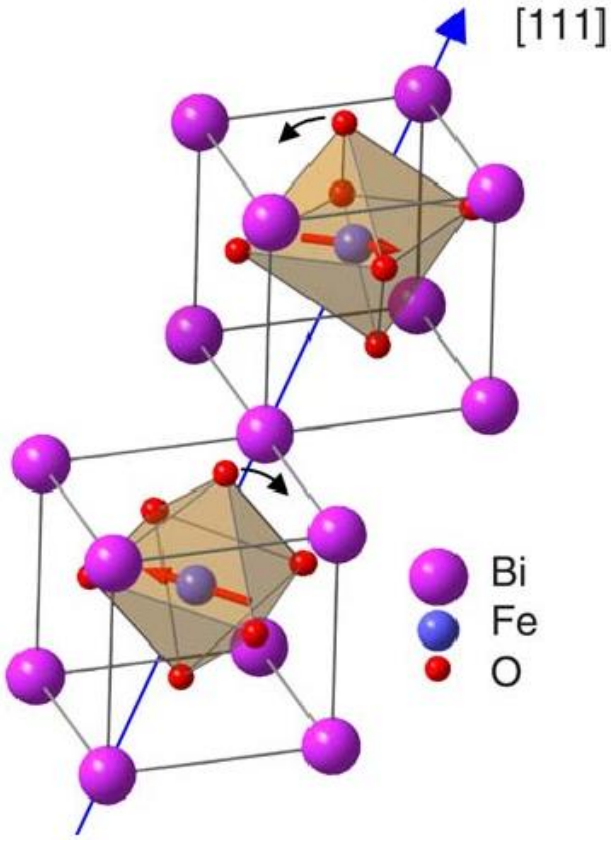

Figure 1.9 Crystal structure of bulk $BiFeO_3$ at room temperature: Two simple perovskite unit cell are shown to illustrate that the successive oxygen octahedron along the polar [111] axis rotate in opposite sense. Arrows on Fe atoms indicate the orientation of the magnetic moments in the (111) plane [after Lubk et al. (2009)].

The hexagonal unit cell shown in Fig. 1.9 consists of six formula units whereas only two formula units are contained in the rhombohedral unit cell generating from anti-phase rotation of adjacent oxygen octahedra about the trigonal $[111]_{pc}$ axis. The symmetry of *R*3*c* space group allows the emergence of a spontaneous electric polarization in the $[111]_{pc}$ direction and a relative shift of Fe, Bi, and O along this three-fold axis [Palewicz et al. (2007)]. Due to highly conducting nature of $BiFeO_3$, the experimental study of its ferroelectric behaviour at room temperature has become a very

challenging task. Because of the leakage current problem, Teague et al. (1970) have performed a measurement of polarisation in the $[111]_{pc}$ polar direction on single crystal of $BiFeO_3$ at liquid nitrogen temperature and reported a rather small value 6.1 $\mu C/cm^2$. This value is significantly lower than the value predicted on the basis of structural point of view. Studies on thin films of bismuth ferrite revealed a very high value of spontaneous polarisation $P_S \sim 150$ $\mu C/cm^2$ [Yun et al. (2004)] and 55 $\mu C/cm^2$ [Wang et al. (2003)] (see Fig. 1.10).

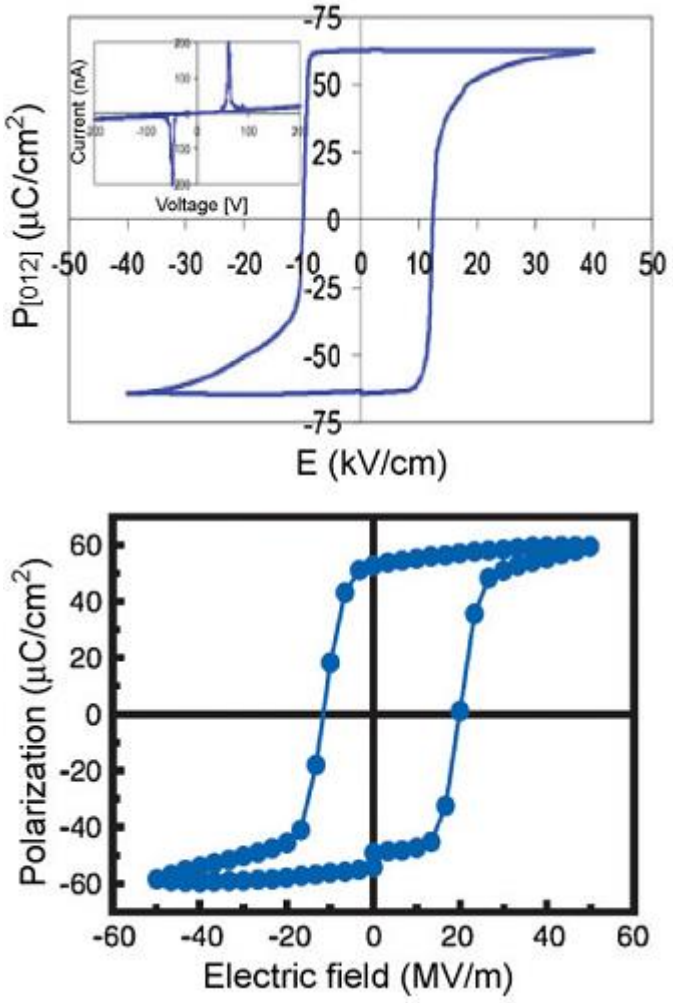

Figure 1.10 Ferroelectric hysteresis loop measured for bulk single crystal (top) and thin film (bottom) grown on (100) oriented substrate $SrTiO_3$ [(after Lebeugle et al. (2007A, 2007 B) & Wang et al. (2003),].

Initially this large value of polarisation obtained from the thin film was expected to come from the strain mediated structural transformation of bulk $BiFeO_3$ from *R*3*c* symmetry to pseudo-tetragonal (strictly speaking monoclinic) symmetry of thin film. First-principles calculations have shown that the spontaneous polarization of even the rhombohedral structure of $BiFeO_3$ can reach 90 - 100 $\mu C/cm^2$ [Neaton et al. (2005); Ravindran et al. (2006)]. More recently, polarization value as high as 100 $\mu C/cm^2$ measured in the direction of polar axis $[111]_{pc}$ has been reported [Lebeugle et al. (2007A)] in the single crystal of $BiFeO_3$. The single crystals of $BiFeO_3$ were grown using Bi_2O_3-Fe_2O_3 flux with a low growth temperature of 1123 K. This work shows that the large value of polarisation exhibited by $BiFeO_3$ is its intrinsic feature; instead of a strain mediated phenomena as expected in the case of bismuth ferrite thin films.

Apart from ferroelectric behaviour, $BiFeO_3$ is also known to exhibit an antiferromagnetic ordering. Sosnowska et al. (1982) studied the magnetic structure of $BiFeO_3$ and showed that the magnetic moments of iron ions are coupled together ferromagnetically within the $[111]_{pc}$ planes and antiferromagnetically between the neighbouring planes, as shown in Fig 1.11. This magnetic order corresponds to G-type antiferromagnetic structure with respect to the elementary perovskite cell. If the orientation of Fe^{3+} magnetic moments are normal to $[111]_{pc}$ direction (i.e. in the $(111)_{pc}$ plane), symmetry also allows them to cant each other due to the existence of Dzyaloshinski-Moriya (DM) interaction between them that leads to a macroscopic magnetisation.

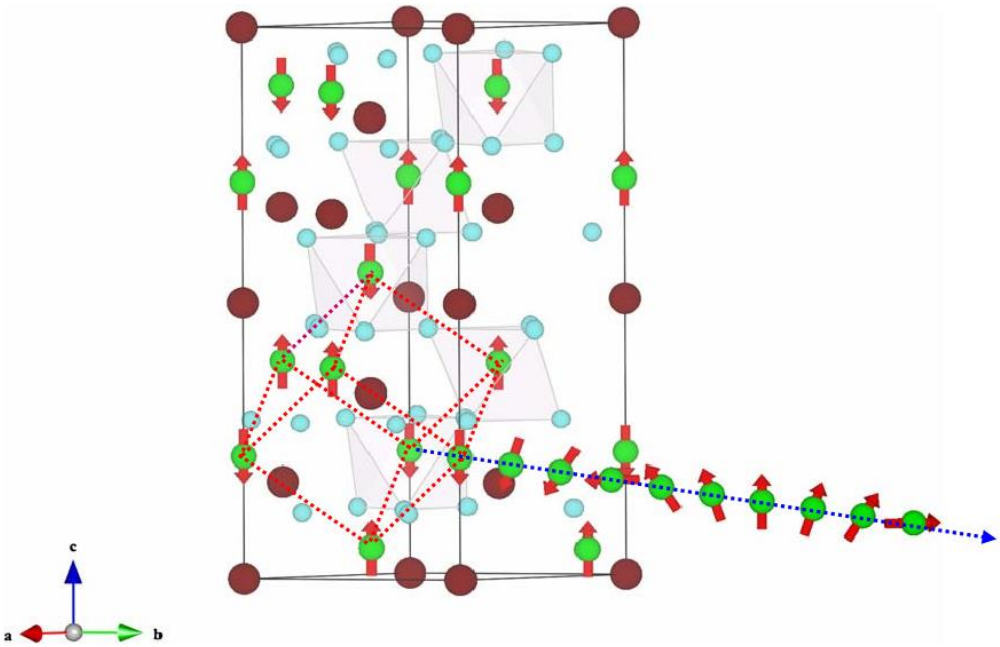

Figure 1.11 $BiFeO_3$ lattice with bismuth (large circles), iron (large circles with arrow) and oxygen ions (small circles) shown in hexagonal settings [after Park et al. (2011)]. The arrow at the Fe sites indicates the direction for magnetic moments. The magnetic cell (dashed lines) is shown for a G-type antiferromagnetic structure. The propagation wave vector of the incommensurate spiral spin structure **k** is along the $[110]_h$ direction and lies in the plane of spin rotation $(1\text{-}10)_h$.

This macroscopic magnetism is termed as weak ferromagnetism. However, it was also found that the orientations of magnetic moments are not spatially similar but rather they comprise a modulated spin spiral structure that is superimposed on the G-type antiferromagnetic ordering. The period of this spiral spin structure was reported of the order of 62nm. In this spiral structure magnetic moments (spins) rotate on $(1\text{-}10)_h$ plane while the modulation wave vector is along $[110]_h$ direction (see Fig. 1.11) [Sosnowaska et al. (1982)]. The presence of modulated spiral spin ordering in bismuth ferrite has also been supported by experimental evidences from NMR [Zalessky et al. (2000); Kozheev et al. (2003)] and EPR [Ruette et al. (2004)]. The arrangement of spins

in this spiral is in such a way that any resultant macroscopic magnetisation over its complete cycle becomes zero.

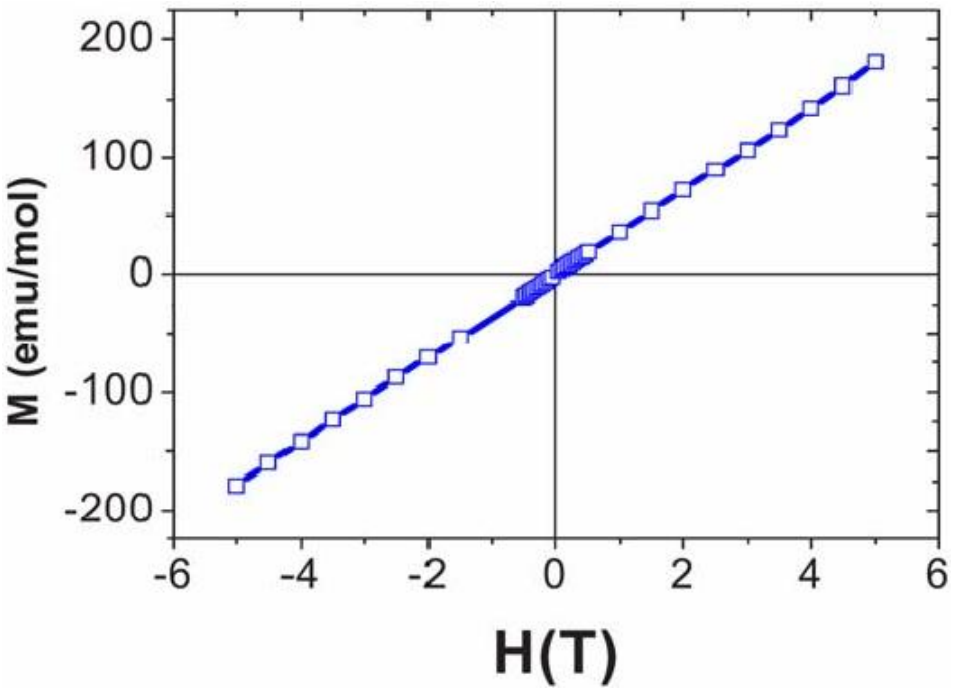

Figure 1.12 Magnetization curve versus applied magnetic field of the powder sample measured at room temperature [after Lebeugle et al. (2007B)].

This is the reason why the measurement of magnetisation (M) as a function of magnetic field (H) and temperature (T) reveals a pure antiferromagnetic response in pure $BiFeO_3$ single crystal [Lebeugle et al. (2007 B)] as shown in Fig. 1.12. Weak ferromagnetism reported in pure $BiFeO_3$ samples in polycrystalline form [Zhang et al. (2005)] is mostly due to the presence of some magnetic impurity.

1.11 Magnetoelectric Coupling in $BiFeO_3$

The presence of spatially modulated spiral spin structure inhibits linear magnetoelectric (ME) coupling in $BiFeO_3$ but it can exhibit quadratic effect [Schmid (1994)] which is quite weak. Due to the presence of spiral spin structure, $BiFeO_3$ does not exhibit any macroscopic magnetization and linear magnetoelectric coupling.

Therefore it is necessary to destroy the spiral spin structure for the release of latent magnetisation and the appearance of linear magnetoelectric coupling. In past, relationship between ferroelectric polarization and antiferromagnetism in insulating $BiFeO_3$ single crystals has been explored in detail using high resolution neutron diffraction by two independent groups [Lebeugle et al. (2008) and Lee et al. (2008 B)]. They have shown that on the application of an electric field, which changes the direction of polarization from one of the $<111>_{pc}$ direction to another, the direction of propagation vector of spiral spin structure also changes (see Fig. 1.13).

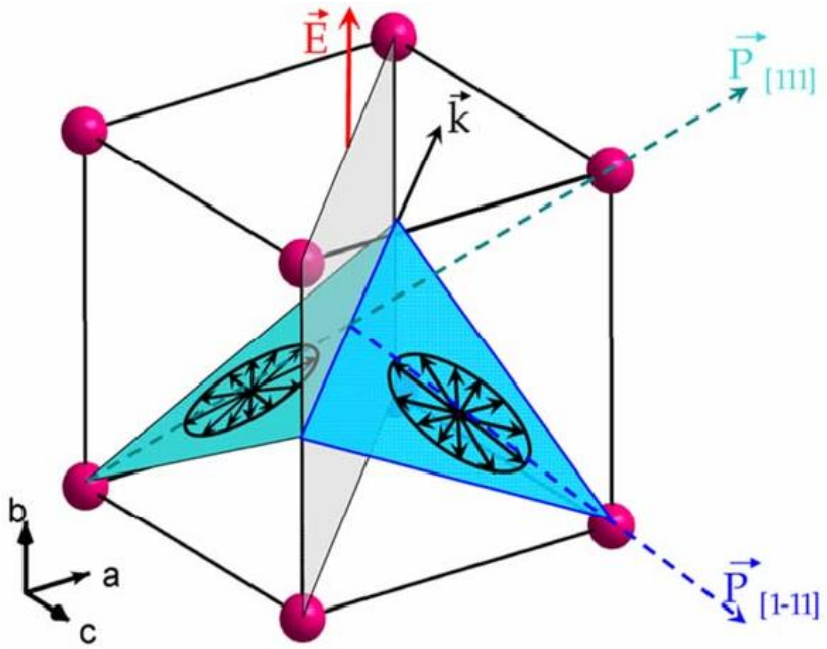

Figure 1.13 Schematic of the planes of spiral rotation and cycloids **k** vector for polarization domains separated by a domain wall [after Lebeugle et al. (2008)].

This experimental observation confirms that the ferroelectric and magnetic orders are indeed coupled in $BiFeO_3$. Various methods have been described in literatures for the destruction of spiral spin magnetic structure present in pure crystal of $BiFeO_3$ as discussed in the following sections.

1.11.1 Effect of Application of High Magnetic Field on $BiFeO_3$

Fig. 1.14 depicts the variation of electric polarisation as a function of applied magnetic field pointed along [001] axis. At $H < H_c$ electric polarisation is essentially quadratic function of magnetic field. However, on increasing the magnetic field above $H = H_c \sim 200$ kOe, the spatially modulated spiral spin structure is destroyed and leads to a remnant magnetization as shown in Fig. 1.14(b). Above the critical field $H_c \sim 200$kOe, the electric polarization changes sign and becomes linearly dependent on magnetic field [Popov et al. (1993)]. This experiment has conclusively established that linear magnetoelectric coupling in $BiFeO_3$ can be observed by the destruction of the spatially modulated spiral spin structure leading to a homogeneous canted G-type antiferromagnetic structure. The absence of linear magnetoelectric coupling in bismuth ferrite has been experimentally established by several other workers also [Tabares-Munoz et al. (1985); Kadomtseva et al. (2004)] for fields below H_C.

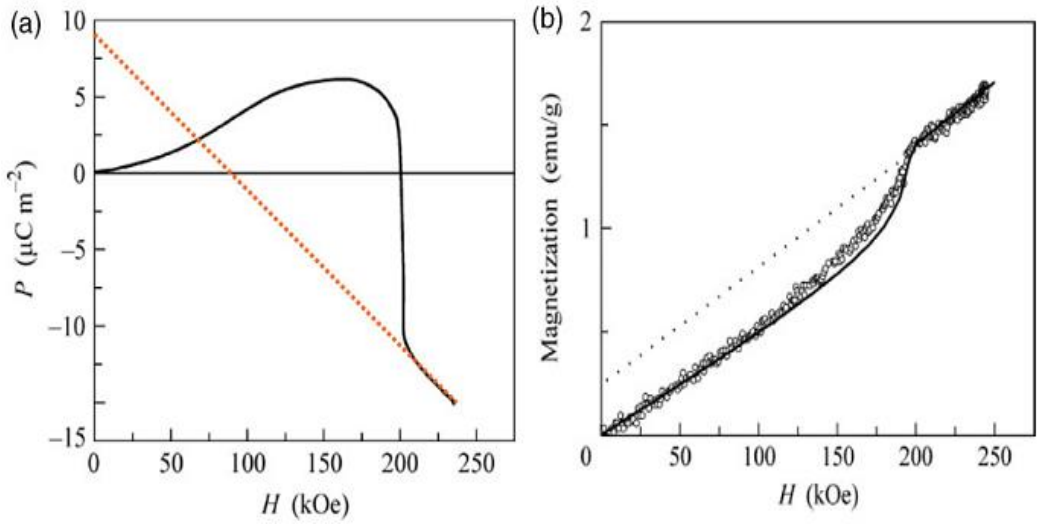

Figure 1.14 (a) Electric polarization (P) induced by magnetic field in $BiFeO_3$ at 10 K [Popov et al. (1993)]. At low fields, P is proportional to H^2, (quadratic ME coupling). Above $H_c = 200$ kOe, P is linearly dependent on H. (b) Magnetization as a function of the magnetic field oriented along the $[001]_c$ (cubic) direction for $BiFeO_3$ at 10 K [after Zvezdin et al. (2006)].

Recently, a microscopic study has been performed by Bordács et al. (2018) on $BieFO_3$ single crystal using small angle neutron scattering (SANS) with and without application of external magnetic field and it was reported that, not only cycloidal domains in $BiFeO_3$ rearrange them on the application of magnetic field, but also for in-plane fields with magnitude ≥ 7 Tesla, only those domains survive that are favoured by the external field. Further, it was also proposed that if in the absence of magnetic field propagation vector of cycloid is not directed perpendicular to the field, they starts to rotate to attain a 90^0 orientation with the field above ≥ 5T. On the basis of such rotation of the cycloid propagation vector subjected to magnetic field, a new mechanism of the coupling between the magnetic anisotropy and the polarization was proposed that further describes the cause of magnetoelectric polarization normal to the rhombohedral axis.

1.11.2 Effect of Chemical Substitutions at Bi and Fe-sites in $BiFeO_3$

In recent years, attempts have been made to synthesize phase pure $BiFeO_3$ based solid solutions with a view to destruct the spiral magnetic structure and improve the ferroelectric properties as well by increasing the resistivity. For example, in the $BiFe_{1-x}Mn_xO_3$ system, using high resolution neutron powder diffraction (NPD) studies, it has been shown that the spiral magnetic structure of $BiFeO_3$ is suppressed towards an ordered antiferromagnetic structure above x = 0.2 concentration (see Fig. 1.15) [Sosnowska et al. (2002)]. In the $0.55(Bi_{0.8}La_{0.2})(Fe,Ga)O_3$-45%$PbTiO_3$ system, remnant magnetizations of ~ 0.15 emu/g and 0.3 emu/g have been proposed at room temperature and 5 K respectively [Wang et al. (2005)]. The value of remnant magnetization (M_r) observed in $0.55(Bi_{0.8}La_{0.2})(Fe,Ga)O_3$-45%$PbTiO_3$ system at low temperature is nearly equal to that for pure $BiFeO_3$ at 10 K under high magnetic field. These results suggest that solid solution formation of bismuth ferrite with other systems

can be a good option to suppress the spiral spin structure and to improve its magnetic as well as electrical properties. The suppression of spiral spin structure with a non-zero remnant magnetization has been observed in several other compositionally modified $BiFeO_3$ solid solutions. Dopants like Ba^{2+}, Pb^{2+}, Sr^{2+} and Ca^{2+} at the A-site have different radius than the Bi^{3+} ion in $BiFeO_3$ and hence they cause an effective destruction of its modulated spiral spin structure leading to the net macroscopic magnetization [Khomchenko et al. (2008)]. The appearance of the remnant magnetization resulting from the destruction of spiral spin structure in $BiFeO_3$-based solids solutions was also predicated theoretically using first principles calculations on La-doped $BiFeO_3$ [Lee et al. (2010)].

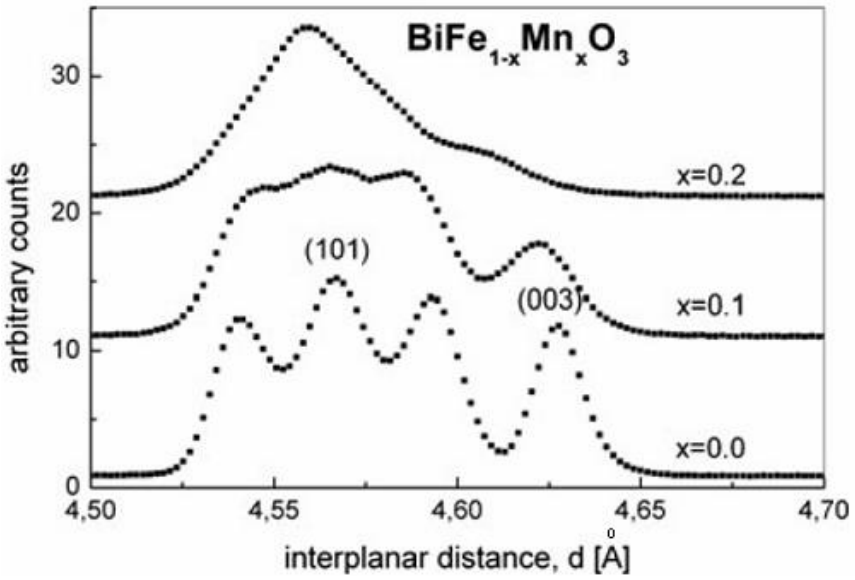

Figure 1.15 Characteristic magnetic satellite reflections for $BiMn_xFe_{1-x}O_3$ measured using OSIRIS diffractometer at ISIS [after Sosnowska et al. (2002)].

Apart from the enhanced multiferroic properties of $BiFeO_3$ based solid solutions system, they also show various crystallographic transformations and interesting phenomenon with increasing concentration of the alloying components [Bhattachrjee et

al. (2010)(B); Rusakov et al. (2011)]. The solid solutions of $BiFeO_3$ with many other perovskite oxides such as $Pb(Fe_{1/2}Nb_{1/2})O_3$ [Kiselev et al. (1969), Patel et al. (2013), Bochenek et al. (2017), Stoch et al. (2018)], $PbZrO_3$ [Ivanov et al. (2008)], $Pb(Zr_xTi_{1-x})O_3$ [Korchagina et al. (2009); Choudhary et al. (2009)], $(Pb,La)(Zr_xTi_{1-x})O_3$ [Kanai et al. (2001)], $BaTiO_3$ [Kumar et al. (2000), Singh et al. (2014), Singh et al. (2013)], $PbTiO_3$ [Zhu et al. (2008); Bhattacharjee et al. (2010)(A &B)], $BiCoO_3$ [Dieguez et al. (2011)], $NaNbO_3$ [Raevski et al. (2008)] and $BiMnO_3$ [Palova et al. (2010)] have been reported.

1.11.3 Magnetoelectricity in Thin Films of $BiFeO_3$

It was found that the modulated spiral magnetic structure of $BiFeO_3$ get modified under epitaxial constraints [Eerenstein et al. (2005)] stimulating magnetic response from $BiFeO_3$. The saturation magnetization (M_s) in epitaxial films of $BiFeO_3$ was reported to be thickness independent with the maximum value of $M_S \sim 0.06\ \mu_B$/Fe Typical M-H response for thin film of $BiFeO_3$ reported by Eerenstein et al. (2005) is shown in inset to Fig. 1.16. Using experimental results, Eerenstein et al. (2005)also ruled out the strain enhanced magnetization reported earlier by Wang et al. (2003). The high value of M_s is attributed to the presence of Fe^{2+} ions in epitaxial films of $BiFeO_3$.

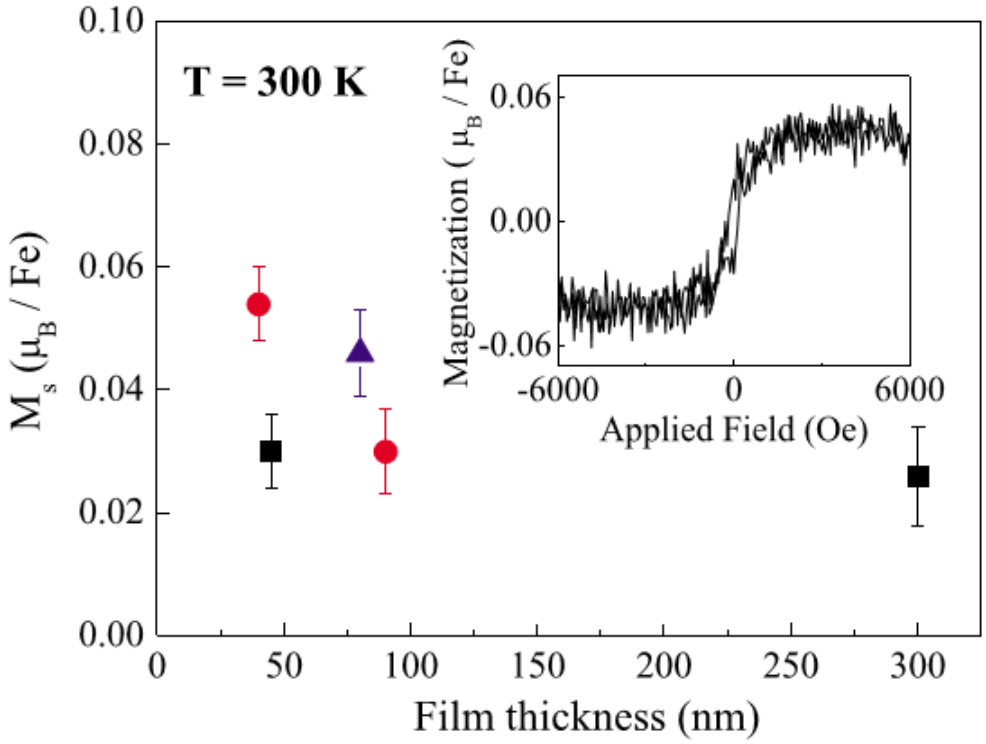

Figure 1.16 Saturation magnetization Ms of $BiFeO_3$ films for various film thickness. Black squares, on $SrTiO_3$ substrate; red circles, $BiFeO_3$/ $SrRuO_3$ (50 nm)/ $SrTiO_3$; blue triangle, $BiFeO_3$/Nb-$SrTiO_3$. The inset shows a typical hysteresis loop. Magnetometer axis in-plane and parallel to $SrTiO_3$ [100] after Eerenstein et al. (2005).

1.11.4 Magnetoelectricity in $BiFeO_3$ by reducing Particle Size

The suppression of modulated spiral spin structure in $BiFeO_3$ and appearance of appreciable value of saturation magnetization (M_S) by the reduction of particle size has been reported by different workers [Majumder et al. (2007), Park et al. (2007)]. Majumder et al. (2007) have obtained saturation magnetization value of ~ 0.40 μ_B/Fe for nanoparticles of $BiFeO_3$ in particle size range 4 - 40 nm, whereas in bulk form M_S is only ~ 0.024 μ_B/Fe. Park et al. (2007) explained the enhancement of the magnetic properties of $BiFeO_3$ by reducing particle size to be due to the enhanced suppression of the spiral spin structure and uncompensated magnetic moments and strain anisotropy at the surface. They have reported that $BiFeO_3$ starts responding magnetically when

particle size reduced below to 95nm and the strength of magnetic respond enhances rapidly for samples with particle size less than 62nm (i.e. when particle size become less than the periodicity of spiral spin structure). Hysteresis loops reported by Park et al. at room temperature for nanoparticles of $BiFeO_3$ for different particle sizes are shown in Fig.1.17 where, inset depicts the variation of magnetization with size of as–prepared $BiFeO_3$ nano-particles at 50 kOe.

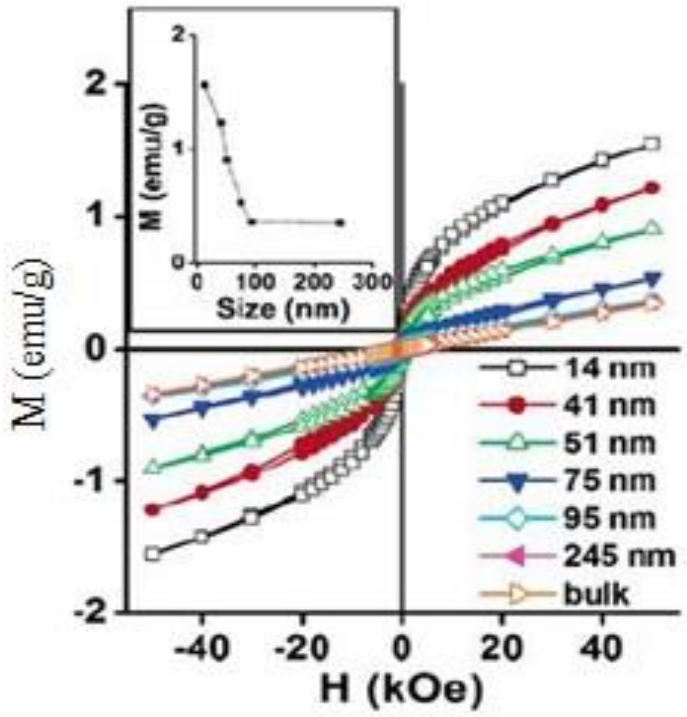

Figure 1.17 Hysteresis loops at 300 K for $BiFeO_3$ nanoparticles with different particle sizes. The inset shows the variation of magnetization of $BiFeO_3$ nano-particles as a function of size (diameter d) at 50 kOe [after Park et al. (2007)].

1.12 Coupling between Polarization, Octahedral Rotation, and Antiferromagnetic Order in $BiFeO_3$ Thin Films Subjected to Electric Field

Electric field (E) does not directly interact with the cycloid spins structure of $BiFeO_3$. To understand the magnetoelectric coupling in $BiFeO_3$ one needs the attention to spin-orbit coupling also. This type of effect is originated from the dependency of

electric polarisation (P) and anti-phase rotation (ω) of oxygen octahedrons in bismuth ferrite unit cell on applied electric field (E). Polarization (P) in $BiFeO_3$ is governed by the energy of spin-flexoelectric interaction [Zvezdin et al (2012)], and anti-phase tilting (ω) of oxygen octahedrons contributing to the magnetic anisotropy energy. In view of the above, the question of how to determine the dependency of (P) and (ω) on electric field (E) arises. Number of mechanisms has been proposed for the investigation of physical manifestations caused by the couplings of these multiferroic parameters [Catalan and Scott (2009), Tagantsev et al. (2001), Goto et al. (2004), Morozovska et al. (2015)]. Using ab-initio method, the effect of electric field (E) on the phase transition in magnetoelectric $BiFeO_3$ has been investigated in seminal work of Lisenkov et al. (2009) that revealed the role of couplings of polarisation (P) and tilt angle (ω) in such processes. However, application of *ab initio* methods to study the transitions of magnetic structures including magnetic spiral, whose scale significantly exceeds the simulation cell size in general, is difficult task. So, a new *ab initio* method has been proposed [Kurz et al. (2004)] for the analysis of both the nonlocal and non-collinear magnetic structures.

To discover the P-ω-L coupling (where, L is an antiferromagnetic order parameter) in the presence of an electric field, Popkov et al. (2015) considered the modified Landau-Ginsburg potential whose phenomenological parameters were obtained by fitting to the data calculated from *ab initio* method [Lisenkov et al. (2009)] and available experiments. In this way they determined the dependency of (P) and (ω) on applied electric field by minimizing, thus constructed, Landau-Ginsburg-like thermodynamic potential. The orientations of antiferromagnetic order parameters (L) in a cycloid were determined from the nonlinear Euler-Lagrange equations whose parameters depend on (E) through the dependency of (P) and (ω) on E. They consider

the uniqueness of the ferroelectric transitions induced by electric field and the related transformations of space-modulated structure. One of the interesting results of this analysis is a sharp reorientation of cycloid plane at the electric field $E_c \approx 60$kV/cm. The variation of electric field induced polarisation (P) and oxygen octahedron tilt angle (ω) as obtained by [Popkov et al. (2015)] is given in Fig. 1.18 (a) and (b) respectively.

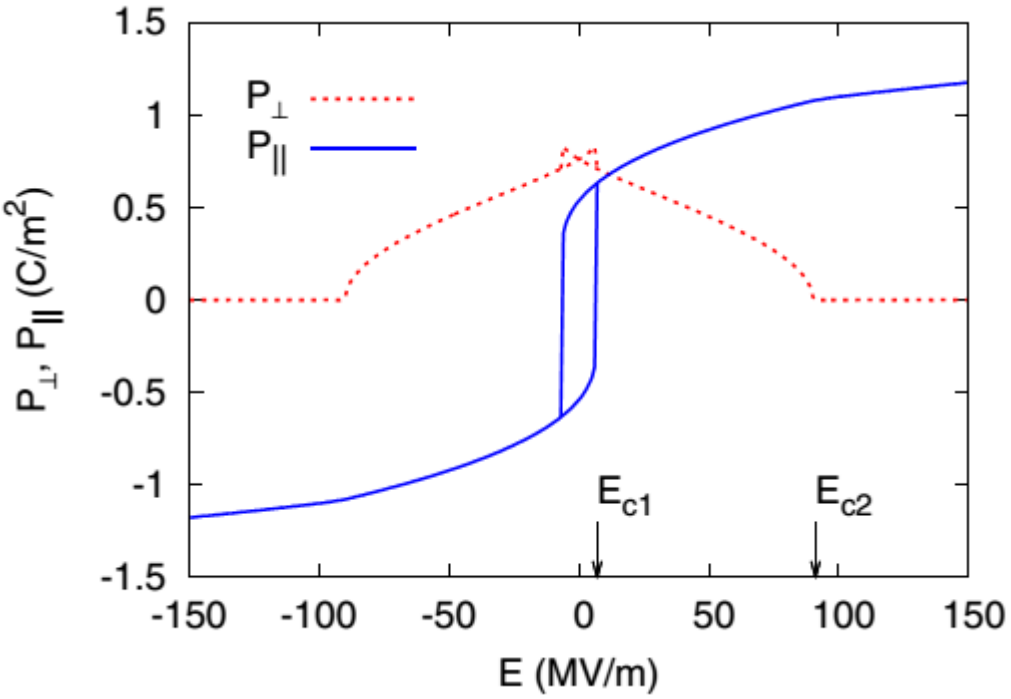

Figure 1.18(a) Electric field (E) dependence of polarization components obtained for E parallel to [001] [after Popkov et al. (2015)].

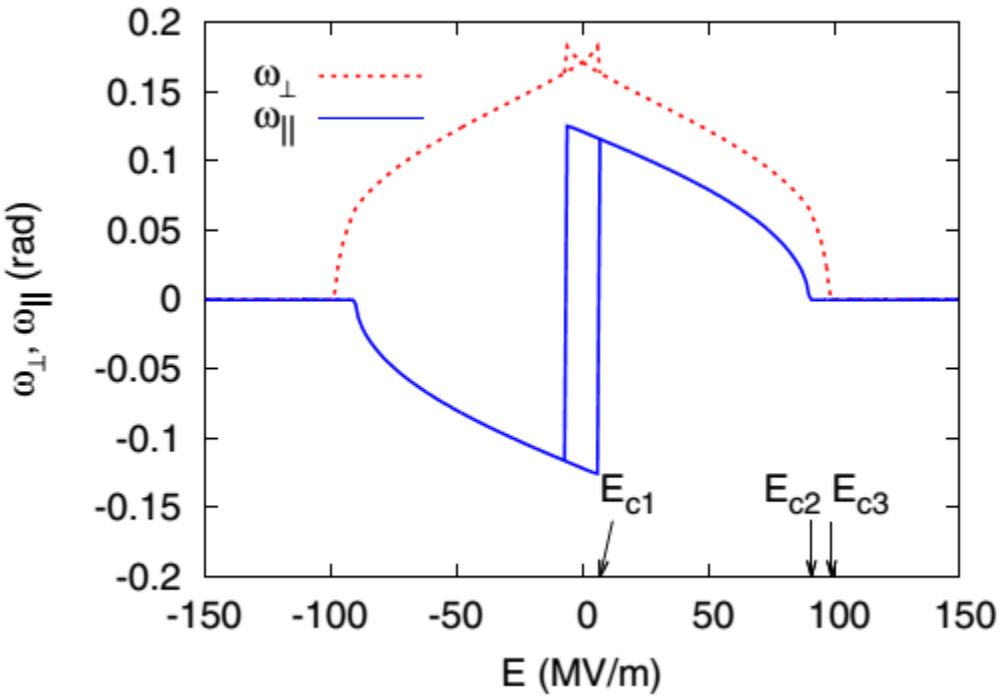

Figure 1.18(b) Electric field (E) dependence of antiferrodistortive vector (ω) components obtained for E parallel to [001] [after Popkov et al. (2015)].

1.13 Low Temperature Phase Transition in $BiFeO_3$

In addition to the antiferromagnetic (T_N) and ferroelectric (T_C) transitions in the region of high temperatures, $BiFeO_3$ is reported to show a number of transitions in low temperature regions [Redfern et al. (2008), Singh et al. (2008B), Ramachandran and Rao (2009)]. Temperature dependent study of $BiFeO_3$ in the low temperature region by measuring the intensity of phonon frequencies by Raman scattering [Singh et al. (2008A), Cazayous et al. (2008), Rovillain et al. (2009)], the dielectric permittivity and elastic modulus [Redfern et al. (2008)] has been revealed a series of anomalies that are attributed to spin reorientation or spin glass transitions analogous to that reported in the rare earth ortho-ferrites. Moreover, the temperature dependence of magnetic entropy change [Fig. 1.19] shows five anomalies [Ramachandran and Rao (2009)] which are in well agreement with the study of Redfern et al. (2008). The two anomalies at ≈ 250K and ≈ 150K (observed in ZFC and FC M(T) measurements) are reported as an

antiferromagnetic to spin glass transition and spin reorientation while the remaining three anomalies at 223, 178, and 38 K are recognized as phase transitions, which are interpreted as following:

(i) The transition at the temperature (223-230K) is considered as glassy but magnetic and weakly coupled with polarization [Ramachandran and Rao (2009), Redfern et al. (2008)].

(ii) The transition at (178-200K) temperature shows magnetoelastic behaviour that is also weakly coupled to polarisation [Ramachandran and Rao (2009), Redfern et al. (2008)].

(iii) Further, the magnetic transition reported at (38-50K) has glassy nature but comes with the feature of magnetoelectric coupling [Singh et al. (2008B), Redfern et al. (2008)].

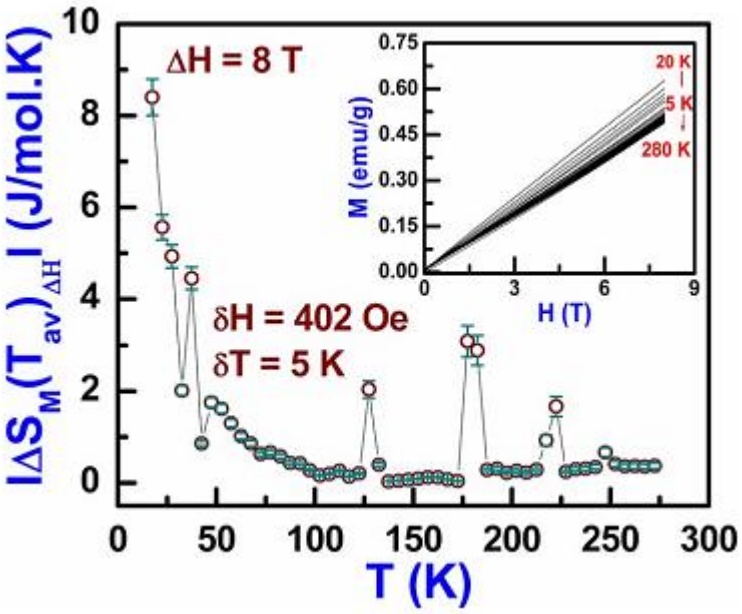

Figure 1.19 The magnetic entropy change versus temperature for polycrystalline $BiFeO_3$ sample. Inset shows magnetization Vs magnetic field of $BiFeO_3$ at high magnetic field (8T) from 15 to 280 K in steps of 5K [after Ramachandran and Rao (2009)].

Initially, Singh et al. (2008A), Cazayous et al. (2008) reported a spin reorientation transition in between the temperatures ≈ 140 and ≈ 210 K that are the temperatures where the spins undergo and complete their rotation. Later on, temperature dependent field cooled (FC) magnetisation measurement [Singh et al. (2008B)] and zero field cooled (ZFC), field cooled (FC) magnetisation and differential scanning calorimetry (DSC) [Ramachandran and Rao (2009)] studies revealed appearance of a spin glass transition below ≈ 250 K. However, neutron diffraction studies did not show any abrupt change in the bulk cycloid structure at the temperatures [Herrero-Albillos et al. (2010), Ramazanoglu et al. (2011) (A), Palewicz et al. (2010)], where these transitions were suggested. Only a gradual but small changes in the periodicity of the spin cycloid was observed [Ramazanoglu et al. (2011A)] while the heat capacity and dielectric permittivity measurements [Lu et al. (2010)] on single crystal as a function of temperature did not show any evidence that support the low temperature phase transitions. These observations suggest that if such transitions occur in $BiFeO_3$, they do not affect the bulk magnetic structure. Temperature dependent study of the data obtained from the grazing-incidence x-ray diffraction measurements also exhibited thermal expansion in the out of-plane lattice parameters between 140 K and 180 K [Jarrier et al. (2012)], which corresponds to the phonon frequency anomaly observed by Raman scattering. In an initial measurement of pyroelectric current, in the zero field cooling regimes, two peaks were observed at ≈140 K and ≈ 210 K while on warming again and measuring the current the only on peak corresponding to ≈ 140 K was seen [Jarrier et al. (2012)]. Further after field cooling, the measurement of pyroelectric current in heating condition and in the absence of field, in addition to 140 K anomaly a broad anomaly at 200 K was also observed [see Fig.1.20].

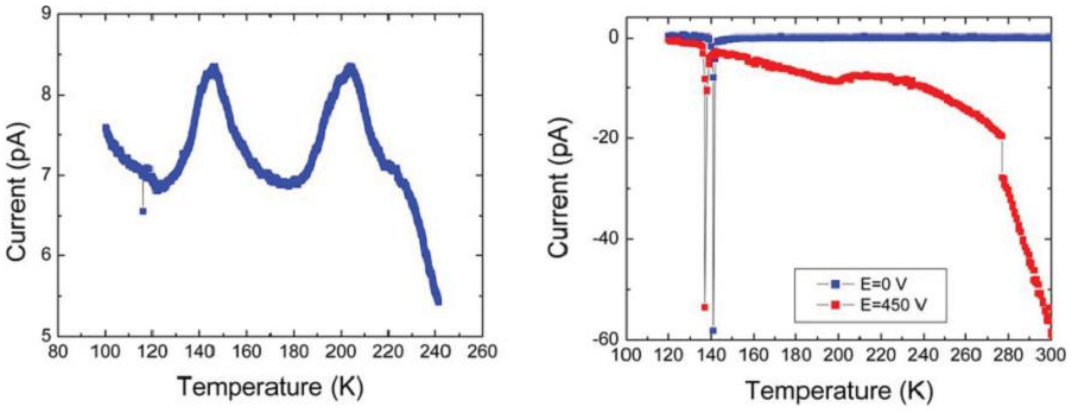

Figure 1.20 Discharge current anomalies in $BiFeO_3$ single crystals. (Left) pristine samples show two clear anomalies at ~ 140 and ~ 200 K, though in subsequent runs (right) only the 140 K anomaly is clear, although the 200 K anomaly is still visible for field-cooled samples. The field-cooling dependence of the peak temperature for the 140 K anomaly indicates that this pyroelectric like current is due to the sudden carrier emission from trap levels triggered by the surface phase transition [after Jarrier et al. (2012)].

The poling history dependent pyroelectric current peak was found to be shifted significantly towards lower temperature region (red curve in Fig 1.20). This shift was attributed to a current originated from the emission of the trapped charges from the forbidden band gap of bismuth ferrite. So the author speculated here that the generation of current was not due to the ferroelectricity but it was due to the injection of charges and thermally stimulated emission from the trapping zone. Further, the structural changes occurring at surface lead to an abrupt change in the Fermi level that allows interfacial defect states to cross above Fermi level and release their charge, leading to sudden jump in current. The experimental evidences from electron paramagnetic resonance (EPR) also support this transition. The EPR result depicted in Fig. 1.21 shows an enhanced asymmetry of the curve, which directly tells about the conductivity of sample, at temperature ≈ 140 K. The EPR data shows a maximum conductivity at ≈

140 K and the results from ab-*initio* calculations performed by the same group shows that bismuth vacancies can generate the required defect levels trapped in the bulk energy gap [Jarrier et al. (2012)].

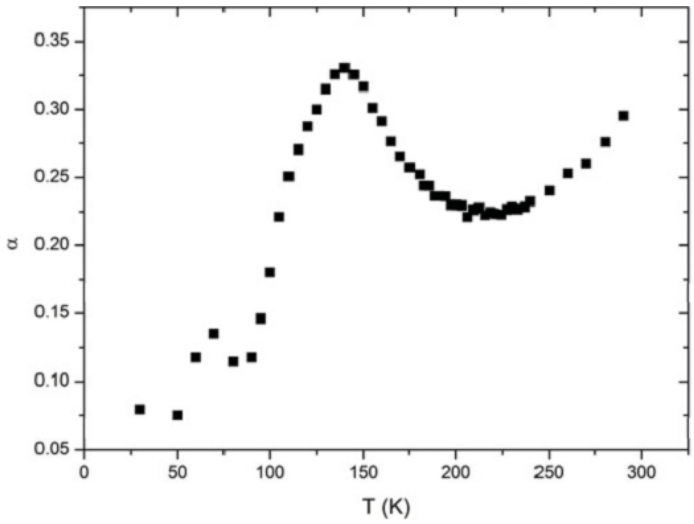

Figure 1.21 Alpha parameter reflecting the asymmetry of the EPR curves for $BiFeO_3$ nanotubes [after Jarrier et al. (2012)].

Thus, the surface phase transition observed around 140 K may be due to the strains imposed by bismuth vacancies in the 'skin'. Extremely high sensitivity of magnetic domains towards uniaxial strains [Ramazanoglu et al. (2011) (B)], may also account for the glassy state between 140 K and 250 K as observed in the temperature dependent magnetisation study [Singh et al. (2008B)]. Recently [Kumar et al. 2018] has reported an experimental evidence for two spin glass transitions in $0.80BiFeO_3$-$0.20BaTiO_3$ system around 30K and 250K using a combination of macroscopic [dc magnetisation M(T), thermo-remnant magnetization M(t), ac susceptibility [$\chi(\omega,T)$] and specific heat (C_p)] and microscopic (x-ray and neutron powder diffraction) measurements. On the basis of these experimental results authors proposed two distinct features of spin glass transitions: (i) the linear variation of unit cell volume strain

(ΔV/V) as a function of square of spontaneous magnetisation revealed the existence of very strong and reasonable magnetoelastic couplings associated with both the spin glass transitions observed around 250K and 30K, respectively, (ii) Presence of strong magnetoelectric effect at both the spin glass transitions as explored by the large change in the calculated spontaneous polarisations using structural data. These two features reported by Kumar et al. 2018 are shown in Fig.1.22 and 1.23 respectively.

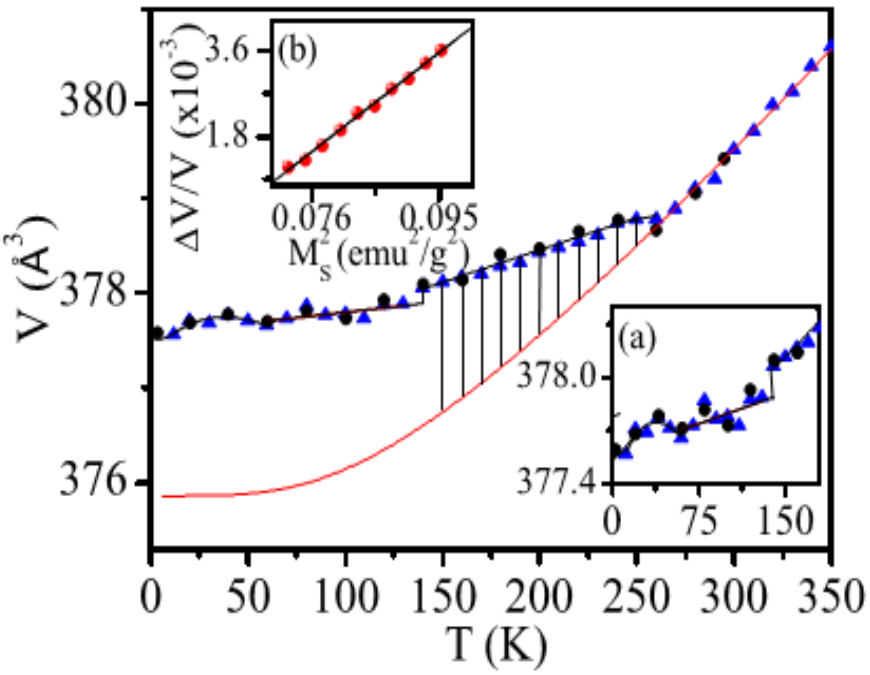

Figure 1.22 Variation of the unit cell volume with temperature for $0.80BiFeO_3$-$0.20BaTiO_3$ ceramic from XRD (▲) and neutron diffraction (●) data. Solid line (-) is fit for Debye Grüneisen equation. Inset (a) shows the zoomed view around 140 K. Inset (b) depicts the variation of volume strain (ΔV /V) against square of magnetization $(M_S)^2$ obtained by M-H measurements [after Kumar et al. (2018)].

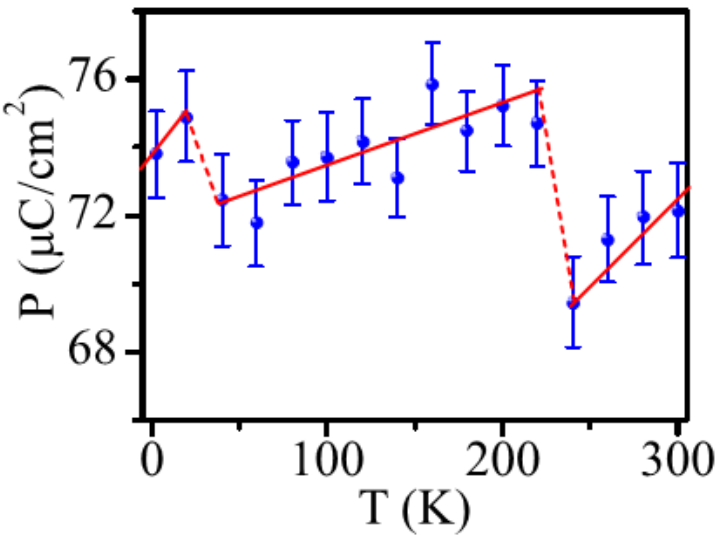

Figure 1.23 Temperature-dependent variation of the spontaneous polarization for $0.80BiFeO_3$-$0.20BaTiO_3$ ceramic calculated from the positional coordinates obtained from Rietveld structure refinement [after Kumar et al. (2018)].

1.14 Crystal Structure and Dielectric Properties of $Sr(Fe_{0.5}Nb_{0.5})O_3$ Ceramic

$Sr(Fe_{0.5}Nb_{0.5})O_3$ (SFN) belongs to the family of perovskites containing iron with general chemical formula $A(Fe_{0.5}B_{0.5})O_3$ where, A = Ba, Sr, Ca and B = Sb, Nb, Ta. Compounds of this class have generally centrosymmetric structure and show giant dielectric permittivity over a broad frequency and temperature range [Chung et al. ((2004) (A), Wang et al. (2013) (A), Raevski et al. (2003), Homes et al. (2001), Saha and Sinha (2002)(A)]. In some of these materials B-site cations arrange itself in a random way and are termed as disordered system. SFN falls in this group of disordered system [Kupriyanov et al. (1962)] in which both the ferromagnetic Fe^{3+} and diamagnetic Nb^{5+} cations are configured in a random manner over the 6-coordinated sites of a pseudo-cubic perovskite structure. The room temperature crystal structure of SFN ceramic is still under debate. At room temperature, various structural models for $Sr(Fe_{0.5}Nb_{0.5})O_3$ (SFN) ceramic have been reported in the literature. [Rodriguez et al. (1985)] have reported cubic structure with lattice parameter 3.987(1) Å for SFN at room

temperature while many authors reported orthorhombic structure in the *Pnma* (*Pbnm*) space group [Tezuka et al. (2000), Liu et al. (2007), Kruea et al. (2013)]. Saha and Sinha (2006) reported monoclinic structure without the specification of space group however; the lattice parameter given by these authors is not consistent with the perovskite lattice parameters which clearly suggest that the structure reported by these authors is incorrect. Saha and Sinha (2006) reported the monoclinic lattice parameters as a = 2.836 Å, b = 2.882 Å, c = 2.804 Å and the monoclinic angle $\beta = 92.83^0$. However, the lattice parameters for primitive perovskite structure are around ~ 4 Å or multiple of it for bigger unit cells. Lufaso et al. (2006) performed Rietveld structure refinement using *I*4/*m* and *I*4/*mcm* space group for SFN having small impurity and concluded that SFN has tetragonal structure in the *I*4/*mcm* space group.

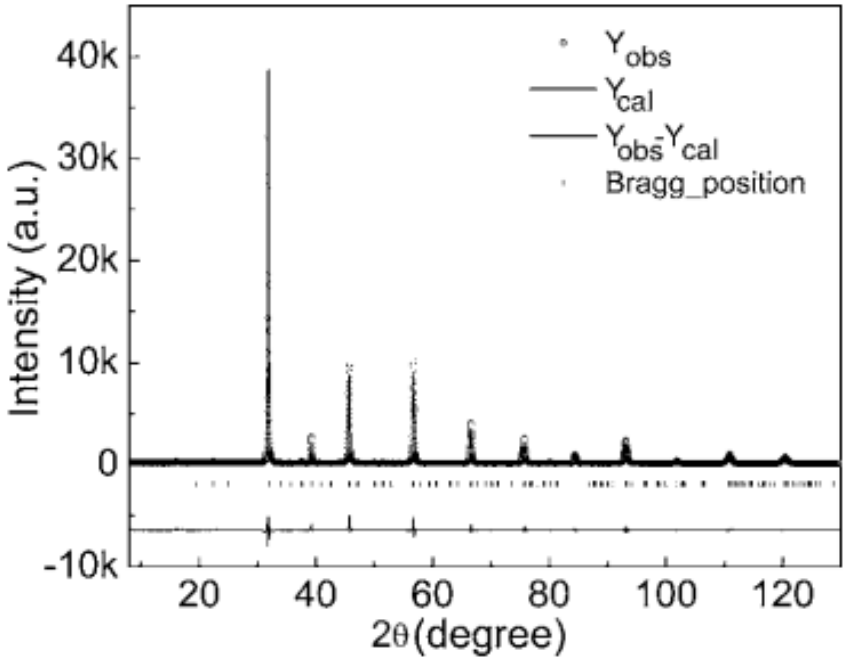

Figure 1.24 Rietveld fit for the x-ray diffraction pattern of $Sr(Fe_{1/2}Nb_{1/2})O_3$ ceramics using orthorhombic crystal structure with *Pbnm* space group [after Liu et al. (2007)].

Later on, using Rietveld structure refinement, Liu et al. (2007) reported that at room temperature SFN crystallizes in orthorhombic symmetry in *Pbnm* space group

with the lattice parameters for SFN at room temperature as a = 5.6120(1) Å, b = 5.6050(1) Å, and c = 7.9616(2) Å. The full pattern refinement fit of the XRD pattern reported by Liu et al. (2007) is shown in Fig. 1.24. This structural model was also followed by Kruea et al. (2013) to study the effect of processing temperature on the various properties of this ceramic. Subsequent to this, by Rietveld structural analysis of XRD data, Akhtar and Khan (2011) reported a tetragonal structure in the *P*4*mm* space group for SFN. The X-ray diffraction pattern reported by them shows clear appearance of superlattice reflection around $2\theta \sim 37.5^0$ [see Fig.1.25] that directly rejects the possibility of *P*4*mm* space group reported by Akhtar and Khan (2011). The controversies on the room temperature crystal structure of SFN ceramic has been resolved by us in the course of present Ph.D. thesis. The results of detailed structural analysis are given in Chapter 3 of this thesis.

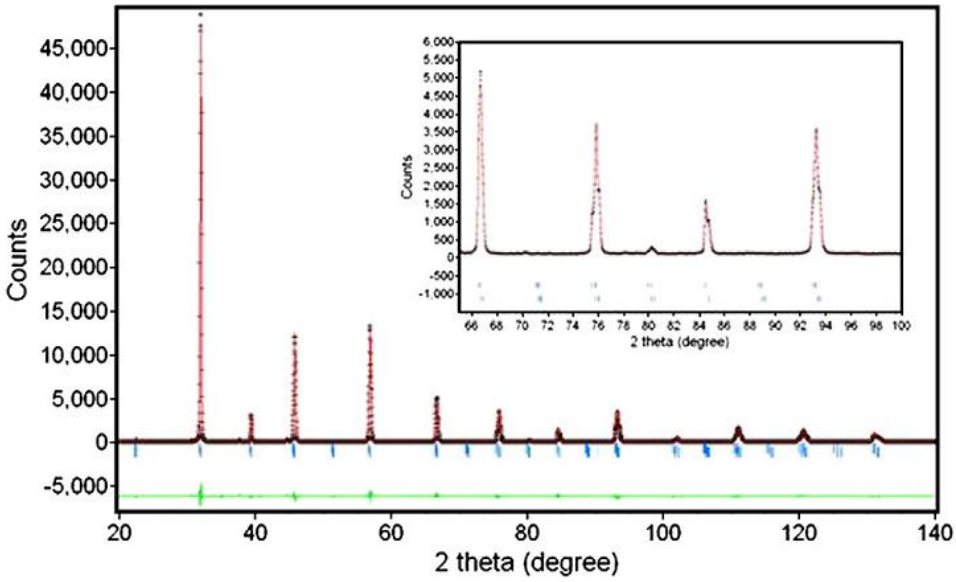

Figure 1.25 Rietveld fit for the x-ray diffraction pattern of $SrFe_{0.5}Nb_{0.5}O_3$; crosses are observed intensities, the red line represents calculated pattern and the lower curve is the difference between observed and calculated XRD patterns. Vertical bars show the reflection positions. Inset highlights fit for $65° \leq 2\theta \leq 100°$ [Akhtar and Khan (2011)].

SFN shows high dielectric permittivity [Raevski et al. (2003)] similar to those reported for $CaCu_3Ti_4O_{12}$ [Li, et al. (2007)]. The work of Saha and Sinha (2006) suggests that the loss (tan δ) and electric modulus (M) spectra of SFN ceramic are nearly temperature independent and the increase of dielectric constant with temperature was attributed to the space charge polarization. In recent study, two dielectric permittivity peaks with strong frequency dependence accompanied with a giant dielectric relaxation step was observed in the as-sintered SFN ceramics, by Liu et al. (2007). Temperature dependent variation of dielectric permittivity (top panel) and loss tangent (tan (δ)) (lower panel) in the frequency range 100Hz to 1MHz are shown in Fig. 1.26. The observed dielectric relaxations were found to be very similar to the previously reported in analogue materials such as $Ba(Fe_{0.5}Nb_{0.5})O_3$ (BFN) [Wang et al. (2007A)] and $Ba(Fe_{0.5}Ta_{0.5})O_3$ (BFT) [Wang et al. (2007B)].

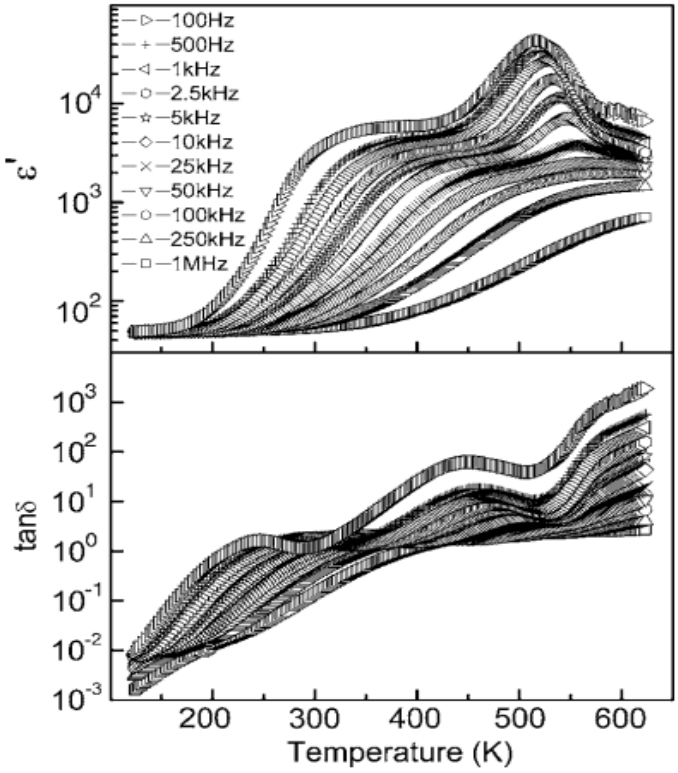

Figure 1.26 Temperature dependence of dielectric constant and dielectric loss for as-sintered $Sr(Fe_{1/2}Nb_{1/2}O_3)$ ceramics at different frequencies [after Liu et al. (2007)].

Liu et al. (2007) have tried to explain the mechanism responsible for the origin of these two dielectric relaxations in the SFN ceramic. To check the behaviour of low and high temperature dielectric relaxation peaks, they annealed the sample in the oxygen atmosphere and measured the dielectric permittivity and loss tangent. The low temperature relaxation step was found to be insensitive to oxygen atmosphere annealing while high temperature relaxor like peak almost completely disappeared (see Fig. 1.27). Due to no evidence for any structural phase transition and change in grain size, the authors attributed these phenomena to the point defects such as V_O, $Fe^{2+}_{Fe^{3+}}$, that are generally formed during sintering in air. The reappearance of high temperature dielectric relaxation (both dielectric constant and dielectric loss peaks) in the O_2-annealed sample after re-annealing in air, confirmed the argument that supports the role of point defect in the SFN ceramic. Therefore, Liu et al. (2007) concluded that the observed low temperature dielectric relaxation step is intrinsic while that observed in high temperature region and sensitive to O_2 annealing is extrinsic. The variation of relaxation temperature with frequency obeys the Arrhenius law with activation energy E_a = 0.38 eV, and pre-exponential factor f_0 = 4.6 ×b 10^9 Hz. They compared the activation energy calculated for SFN ceramic to that reported for similar dielectric relaxation in $LuFe_2O_4$ and proposed that the low temperature dielectric relaxation is a thermally induce intrinsic process and can be attributed to electronic ferroelectricity generated from the charge ordering analogous to $LuFe_2O_4$ [Ikeda et al. (2005)]. It has also been proposed that the giant dielectric relaxation step over a broad temperature range is the consequence of the competing low and high temperature dielectric relaxations.

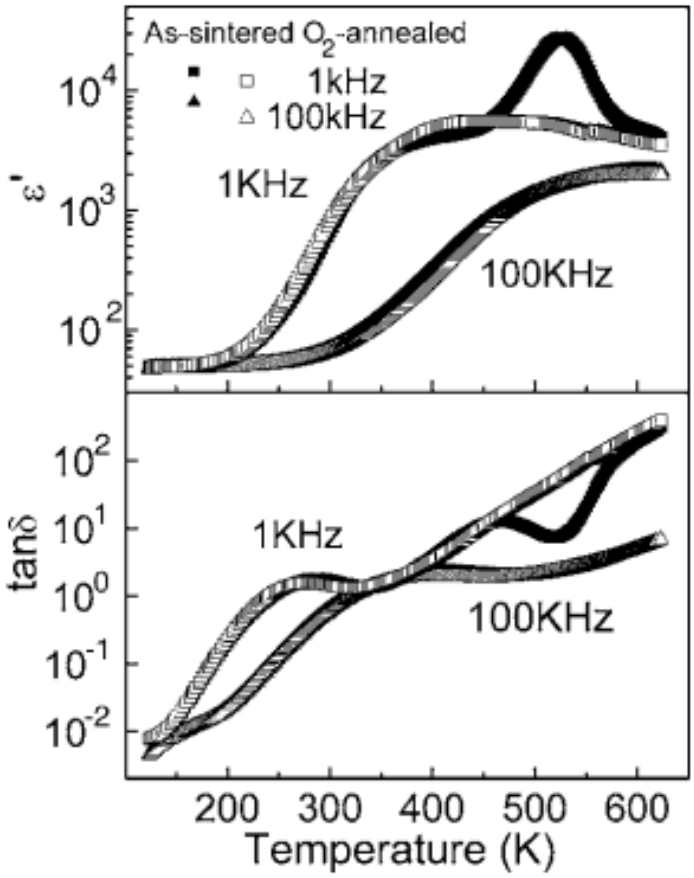

Figure 1.27 Comparison of temperature dependence of dielectric permittivity and dielectric loss for as-sintered and O_2-annealed $Sr(Fe_{1/2}Nb_{1/2})O_3$ ceramics [after Liu et al. (2007)].

1.14.1 Magnetic Phase Transition in $Sr(Fe_{0.5}Nb_{0.5})O_3$

The nature of magnetism and magneto-transport properties of compounds having general formula $A_2B'B''O_6$ (where, A = Sr, Ca, Ba; B′ = Fe, Mn, Cr; B″ = Mo, W, Ta, Nb) are primarily governed by the arrangements related to charge difference and ionic radii of the metal ions occupying B-site [Rama et al. (2004)]. The arrangement (orderly or in a random fashion) of cations occupying B-site in the lattice is determined by their charges as well as ionic radii [Anderson et al. (1993)]. So, the physical properties of such perovskites are governed generally by the arrangements of B-site cations. Various ionic pairs of B′ and B″ in these perovskite exhibit a variety of physical

properties. For example, Sr_2MnMoO_6, Ba_2FeNbO_6, Ba_2MnNbO_6 and Sr_2FeNbO_6 are an antiferromagnetic (AFM) insulator with a T_N of 12 K [3-Itoh et al. (1996)], 25K, 12K [Rama et al. (2004], and 25K [Tezuka et al. (2000), Rama et al. (2004] respectively, while Sr_2FeMoO_6 is a ferromagnetic (FM) metal with a T_C of about 400 K, [2-Kobayashi et al. (1998), 3-Itoh et al. (1996)].

Analysis of magnetic hysteresis loops and temperature dependent dc susceptibility data suggest that Sr_2FeNbO_6 behaves as a spin glass below 32.5 K, [Rodriguez et al. (1985)] and there is no evidence of a transition to a phase showing long-range magnetic order. Further, investigation on magnetic transition in SFN was performed by measuring temperature dependent zero field cooled (ZFC), field cooled (FC) and thermal remnant magnetization (TRM) [Tezuka et al. (2000)] (see Fig 1.28). These experimental results indicate that at the temperatures below ~ 25K, magnetic moments of Fe^{3+} ions align antiferromagnetically with a weak ferromagnetic component that disappear on increasing temperature. On the basis of experimental observations, authors concluded that antiferromagnetic interaction between Fe^{3+} ions survive at low temperatures with a weak ferromagnetic components bellow Neel temperature (T_N). The results reported by [Tezuka et al. (2000)] contradict previously reported one that predicts, SFN does not show any magnetic transition above 32.2 K but show glassy nature below that temperature and such behaviour was attributed to short range structural ordering of Fe^{3+} and Nb^{5+} [Rodriguez et al. (1985)]. However, subsequent EXAFS and Mossbauer studies failed to find any evidence for such a short-range structural ordering [Gibb and Whitehead (1993)].

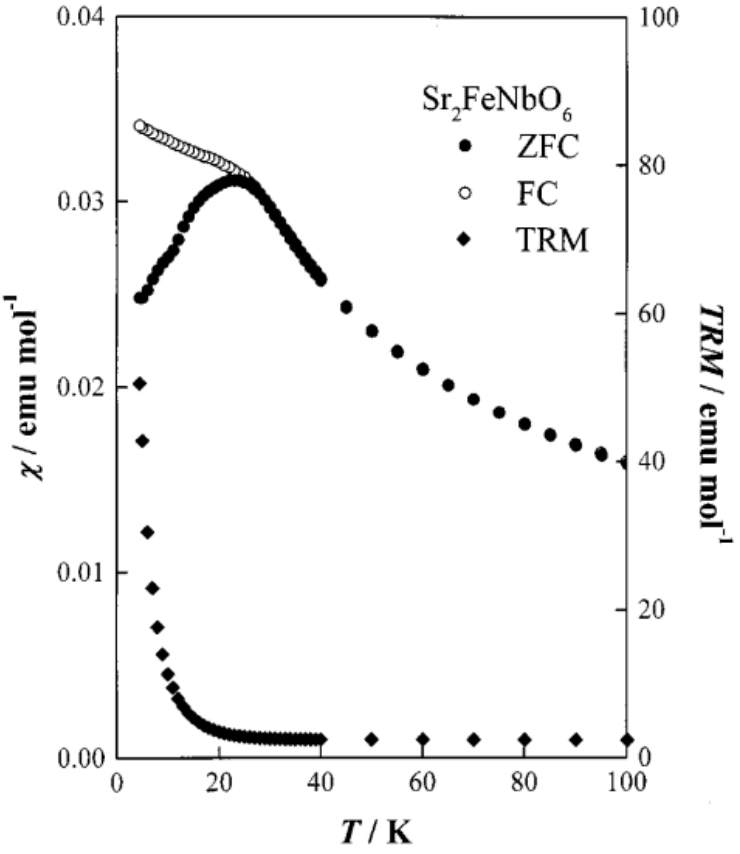

Figure 1.28 Temperature dependence of the ZFC and FC magnetic susceptibilities for Sr_2FeNbO_6. The temperature dependence of the thermal remnant magnetization (TRM) is also shown [after Tezuka et al. (2000)].

Moreover, [Rama et al. (2004)] have studied the changes in Neel temperature (T_N) by substituting A-site with different cations (such as Ba^{2+} and ($0.5(Ba^{2+}Sr^{2+})$) and found that Neel temperature is insensitive towards the A-site substitution in these compounds. This can be seen from temperature dependent magnetization plot in [Fig. 1.29]. It has been proposed that such a behaviour is because of the reason that A-site substitution is not able to change the band gap significantly in the perovskite systems having B″ ions such as Nb^{5+} and W^{6+} (nd^0 configuration) [Hank et al. (2003)].

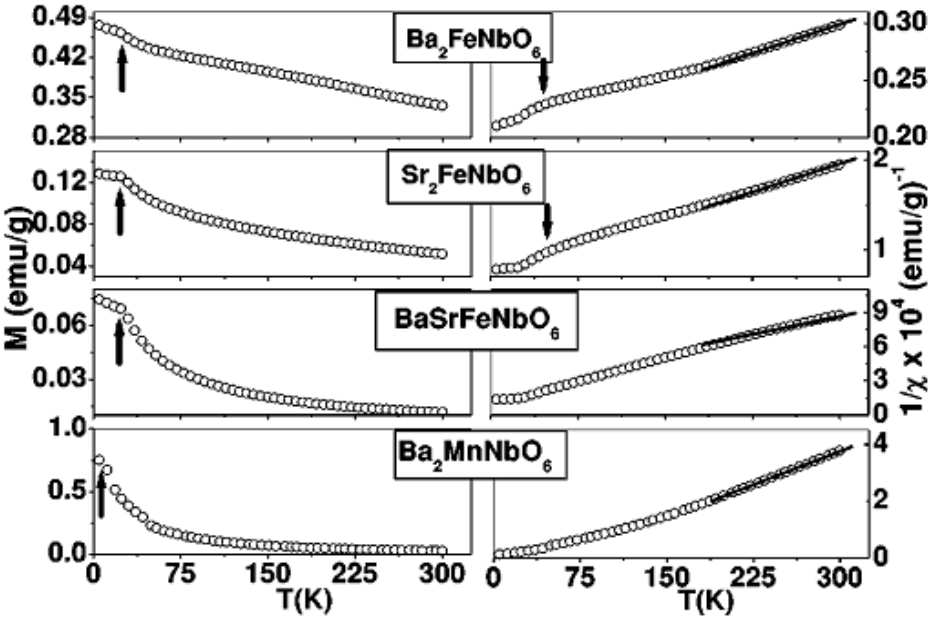

Figure 1.29 Left panel: Magnetization curves of Ba_2FeNbO_6, Sr_2FeNbO_6, $BaSrFeNbO_6$, and Ba_2MnNbO_6. The arrow points to temperature T_N. Right panel: corresponding 1/x vs T plots. The arrow indicates the magnetic correlations above T_N. Solid lines represent the fits to Curie-Weiss law [after Rama et al. (2004)].

1.15 Solid Solutions of $BiFeO_3$ with $Sr(Fe_{0.5}Nb_{0.5})O_3$

To the best of our knowledge no work have been reported in literature on the solid solution system (1-x)$BiFeO_3$-x$Sr(Fe_{0.5}Nb_{0.5})O_3$ (1-x)BF-xSFN. If this system could show good application oriented properties, it will have an advantage over lead-based compounds because the utilization of lead is undesirable from the view point of the actual application due to toxicity of lead. However, a lot of works have been done to investigate structural and magnetic properties in low and high temperature regions, on the analogue compound such as (1-x)$BiFeO_3$-x$Pb(Fe_{0.5}Nb_{0.5})O_3$ [Roginskaya et al. (1966), Bokov et al. (1962), Bhatt et al. (2004), Patel et al. (2010 and 2013),] and on many other one like of (1-x)$BiFeO_3$-x$BaTiO_3$ [Kumar et al. (1998), Kim et al. (2004), Ozaki et al. (2009), Chandarak et al. (2009), Leontsev et al. (2009), Singh et al.

(2008(C), 2011, 2013, 2014)], (1-x)$BiFeO_3$-x$PbTiO_3$ [Reyes et al. (2007), Bhattacharjee and pandey (2010A & 2011)], (1-x)$BiFeO_3$-x$SrTiO_3$ [Vura et al. (2014), Liu et al. (2015)]. By the analysis of X-ray powder diffraction data of (1-x)$BiFeO_3$-x$Pb(Fe_{0.5}Nb_{0.5})O_3$ ceramic Patel et al. (2010 and 2013) have shown that for the compositions $x < 0.35$ crystal structure remains rhombohedral in *R*3*c* space group and for compositions $0.35 \leq x < 0.40$ two coexisting phases, namely, (*R*3*c* + *Pm*-3*m*) were found. They proposed that the phase coexistence suggest that the morphotropic phase boundary is of first order type. In the composition range $0.40 \leq x \leq 0.90$ the evolution of singlet peaks and the absence of superlattice reflections reveals cubic structure with *Pm*-3*m* space group as confirmed by Rietveld structure refinement. For the composition range $0.90 < x \leq 0.96$ monoclinic phase with *Cm* space group was reported. The variation of lattice parameters and unit cell volume as the function of composition reported by Patel et al. (2010 and 2013) is depicted in Fig. 1.30. Singh et al. (2008(C), 2011, 2013, 2014) have studied the room temperature crystal structure of (1-x)$BiFeO_3$-x$BaTiO_3$ ceramic samples in the entire composition range $0.0 \leq x \leq 1.0$. Using X-ray diffraction patterns of powder ceramic sample, they proposed that there exist rhombohedral phase in the *R*3*c* space group for compositions with $x < 0.35$. This rhombohedral phase gradually transforms to a cubic like phase in the *Pm*-3*m* space group around $x_c = 0.35$ that is stable over a wide composition range of $0.35 < x \leq 0.85$.

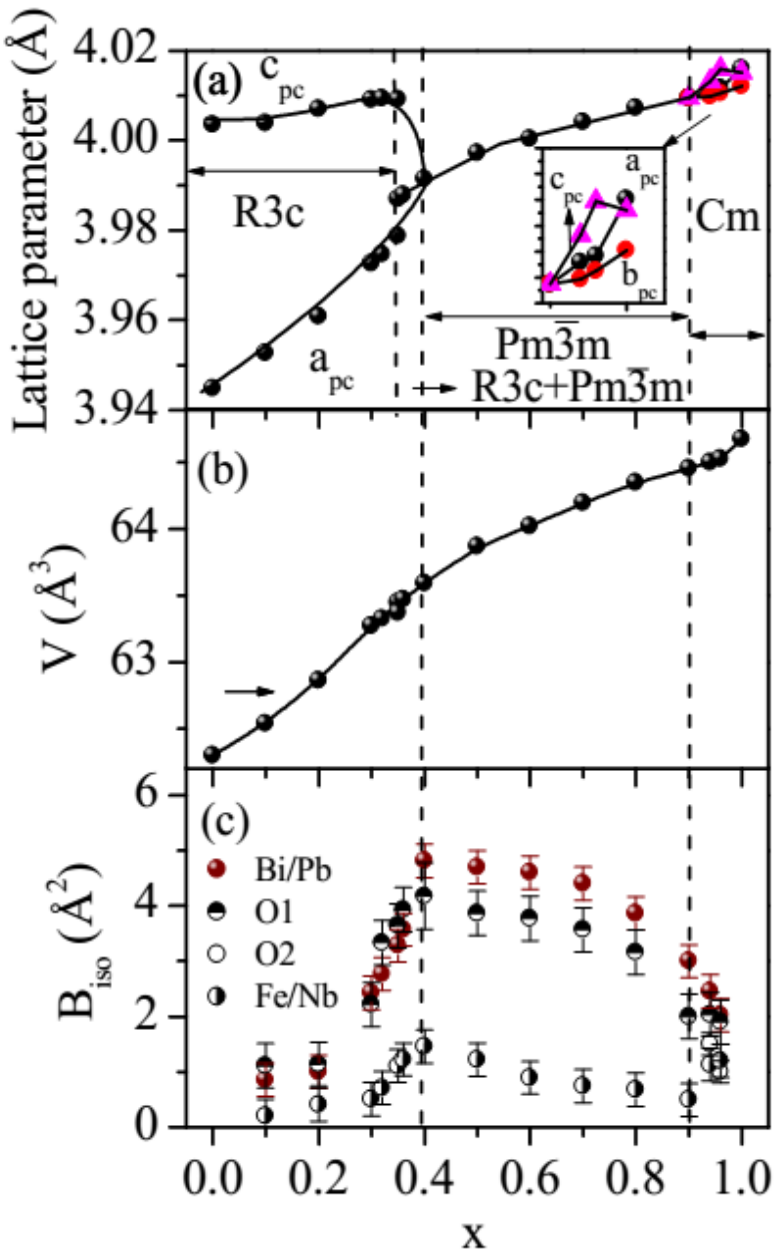

Figure 1.30 Composition dependent variation of (a) refined pseudocubic lattice parameter, (b) pseudocubic unit cell volume (c) isotropic thermal parameters for the Bi^{3+}/Pb^{2+}, O^{2-}andFe^{3+}/Nb^{5+} ions in (1-x)$BiFeO_3$-x$Pb(Fe_{0.5}Nb_{0.5})O_3$ ceramic [after Patel (2014)].

For the compositions with x > 0.85, a tetragonal distortion like characteristic in *P*4*mm* space group appears which gradually approaches the $BaTiO_3$ values for x = 1.00 with increasing x. The variation of unit cell parameters, unit cell volume, pseudo

tetragonality (c/a) and thermal parameters for (1-x)$BiFeO_3$-x$BaTiO_3$ solid solution as a function of composition (x) at room temperature are presented in Fig. 1.31.

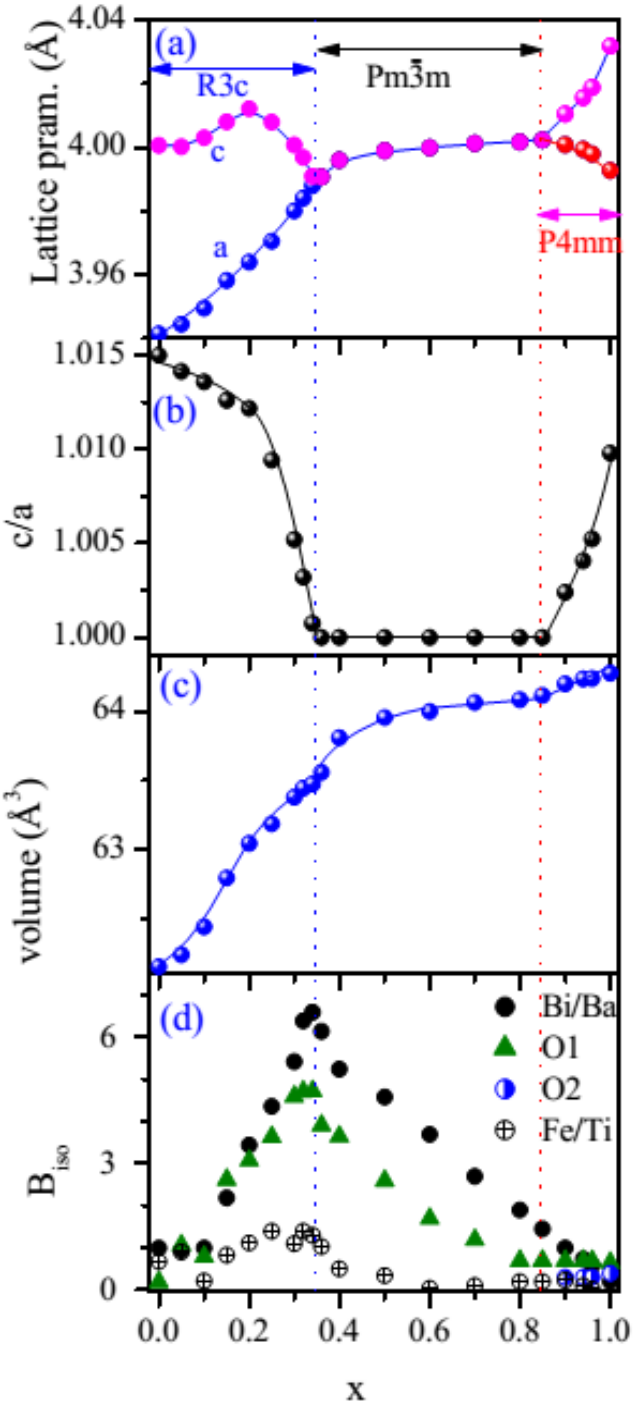

Figure 1.31 Variation of (a) unit cell parameters, (b) pseudo tetragonality (c/a), (c) unit cell volume and (d) thermal parameters in (1-x)$BiFeO_3$-x$BaTiO_3$ as a function of composition (x) at room temperature [after Singh et al. (2013)].

Further Singh et al. (2013) reported that the phase boundaries are qualitatively similar to those reported by Ismailzade et al. (1981) and Kumar et al. (2000) except for the shift in the phase boundaries by ≈ +2% for the rhombohedral to cubic and ≈ -7.5% for cubic to tetragonal transitions. One of the possible reasons of the shift in the structural phase boundaries may be due to the compositional fluctuations by the loss of Bi_2O_3 and formation of unwanted phases in the earlier studies. The most important observations made by Singh et al. (2013) are the high amplitude of thermal parameters for A and O-sites ions. The anomalously high values of thermal parameters indicate the possibility of positional disorder at A and/or O-sites. This positional disorder at A and/or O-sites within the average cubic lattice may lead to the creation of local dipole moments and hence induce ferroelectricity in the so-called cubic phase region $0.35 < x \leq 0.85$.

Bhattacharjee and Pandey (2010A) studied the room temperature crystal structure of $(1-x)BiFeO_3$-$xPbTiO_3$ solid solution in the composition range $0.10 < x \leq 0.90$ by using Rietveld structure refinement from room temperature X-ray powder diffraction data. The crystal structure is reported to be pure monoclinic in the *Cc* space group, and not rhombohedral as proposed by earlier authors [Fedulov et al. (1964), Smith et al. (1968), Zhu et al. (2008)] for the composition range of $0.10 < x \leq 0.27$. In the composition range $0.27 < x < 0.31$ structure was proposed to be the coexistence of two phases, namely, monoclinic phase with *Cc* space group and tetragonal phase in *P*4*mm* space group (*Cc* + *P*4*mm*) as a result of first order character of the morphotropic phase boundary. The Rietveld refinement for the composition $x = 0.31$ was reported to exhibit largest tetragonality which is generally found in Pb-based system. All the compositions with $x > 0.31$ were also reported as tetragonal in *P*4*mm* space group. The variation of lattice parameters as a function of composition as reported by Bhattacharjee and Pandey (2010A) is shown in Fig. 1.32.

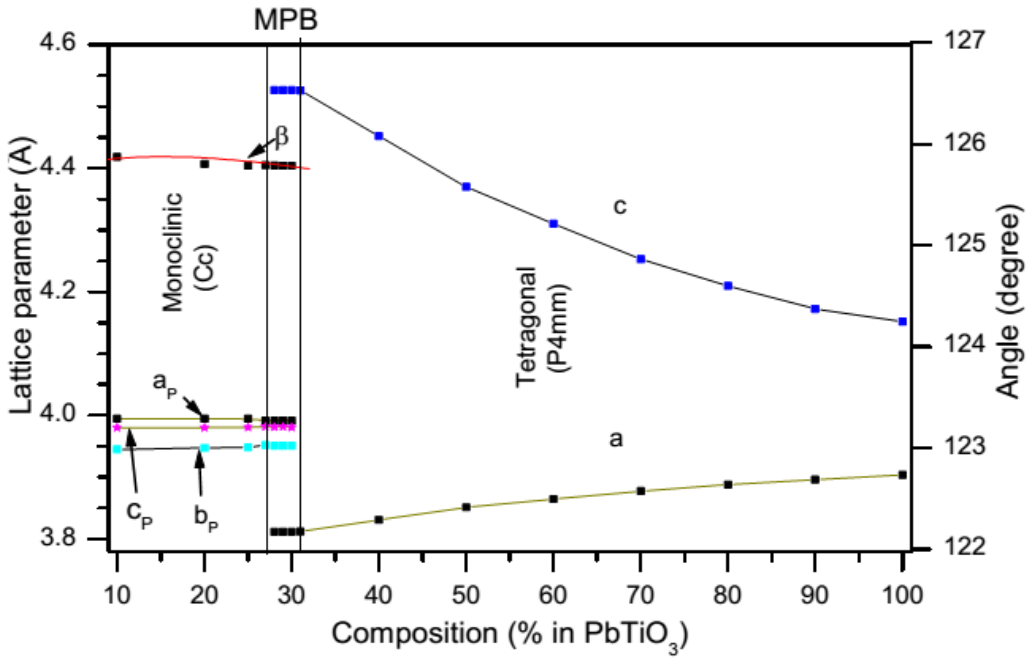

Figure 1.32 Variation of lattice parameters with composition for (1-x)$BiFeO_3$-x$PbTiO_3$ solid solution [after Bhattacharjee and Pandey (2010)A].

1.16 Objectives of the Present Work

As discussed earlier, the (1-x)$BiFeO_3$-x$Sr(Fe_{0.5}Nb_{0.5})O_3$ solid solution system has not been investigated by earlier authors. The main objectives of the present work on are following:

1. To optimize the synthesis conditions and synthesize several compositions of phase pure (1-x)$BiFeO_3$-x$Sr(Fe_{0.5}Nb_{0.5})O_3$ ceramic.

2. To resolve the controversies related to the room temperature crystal structure of $Sr(Fe_{0.5}Nb_{0.5})O_3$ and study the temperature dependent structural and magnetic phase transitions.

3. To investigate the crystal structure and magnetic properties of (1-x)$BiFeO_3$-x$Sr(Fe_{0.5}Nb_{0.5})O_3$ solid solution as a function of composition.

4. To investigate the temperature dependent crystallographic and magnetic phase transitions as well as magnetoelectric coupling in selected compositions of (1-x)$BiFeO_3$-x$Sr(Fe_{0.5}Nb_{0.5})O_3$ solid solution.

The results of the above investigations are described in the subsequent chapters of this thesis.